Development of nanocomposite LSCF perovskite-based cathode material for intermediate temperature solid oxide fuel cells

By

Usman Ashraf

Reg# 00000206572

Session 2017-2019

Supervised by

Prof. Dr. Zuhair S. Khan

A Thesis Submitted to the Centre for Energy Systems in partial fulfillment of the requirements for the degree of

MASTERS of SCIENCE

in

ENERGY SYSTEMS ENGINEERING

U.S.-Pakistan Center for Advanced Studies in Energy

National University of Sciences and Technology (NUST),

H-12, Islamabad 44000, Pakistan

August 2021

THESIS ACCEPTANCE CERTIFICATE

Certified that final copy of MS/MPhil thesis written by <u>Mr Usman Ashraf,</u> (Registration No. <u>00000206572),</u> of <u>USPCAS-E</u> has been vetted by undersigned, found complete in all respects as per NUST Statues/Regulations, is within the similarity indices limit and is accepted as partial fulfillment for the award of MS/MPhil degree. It is further certified that necessary amendments as pointed out by GEC members of the scholar have also been incorporated in the said thesis.

Signature: _____

Name of Supervisor _____ Dr. Zuhair S. Khan _____

Date: _____

Signature (HoD): _____

Date: _____

Signature (Dean/Principal): _____

Date: _____

Certificate

This is to certify that work in this thesis has been carried out by **Mr. Usman Ashraf** and completed under my supervision in Advance Energy Materials Lab, Centre for Energy Systems, National University of Sciences and Technology, H-12, Islamabad, Pakistan.

Supervisor: _____
Dr. Zuhair S. Khan
USPCAS-E
NUST, Islamabad

GEC member # 1:   _____
Dr. Naseem Iqbal
USPCAS-E
NUST, Islamabad

GEC member # 2:   _____
Dr. Nadia Shahzad
USPCAS-E
NUST, Islamabad

GEC member # 3:   _____
Dr. Imran Shahzad
(NCP), Islamabad

HoD-ESE (dept)   _____
Dr. Rabia Liaqat
USPCAS-E
NUST, Islamabad

Principal/Dean   _____
Dr. Adeel Waqas
USPCAS-E
NUST, Islamabad

Dedication

Dedicated to family and friends.

Table of Content

Abstract

Lanthanum strontium cobalt ferrite (La$_{0.6}$Sr$_{0.4}$Co$_{0.2}$Fe$_{0.8}$O$_{3-\delta}$, LSCF), due to its mixed ionic and electronic conductivity, is an important cathode material for intermediate temperature solid oxide fuel cells (IT-SOFCs). In this study, LSCF-GDC nanocomposite cathode for IT-SOFC applications is developed. The LSCF and GDC nanopowders were prepared via solution combustion synthesis method. The nanocomposite cathode material was prepared by mixing LSCF and GDC in 50:50 wt%. The LSCF-GDC nanocomposite cathodes were prepared and sintered at 1100 $^{\circ}$C employing rapid microwave heating. To assess the effects of microwave sintering, LSCF-GDC samples were sintered with conventional resistance heating and compared with the microwave sintered samples. To evaluate the electrical performance of the LSCF-GDC cathode, AC conductivity measurements were performed at temperatures of 300°C to 600°C. Microwave sintered cathode showed a higher electrical conductivity of 0.016 S/cm at 600°C as compared to the conventionally sintered cathode, which was 0.013 S/cm.

Keywords: IT-SOFC, LSCF-GDC nanocomposite, Conventional Sintering, Microwave Sintering

List of Figures

List of Tables

List of Papers/Journals

Microwave-assisted sintering of LSCF-GDC composite based cathode for intermediate temperature solid oxide fuel cells

Lanthanum strontium cobalt ferrite ($La_{0.6}Sr_{0.4}Co_{0.2}Fe_{0.8}O_{3-\delta}$, LSCF), due to its mixed ionic and electronic conductivity, is an important cathode material for intermediate temperature solid oxide fuel cells (IT-SOFCs). However, to compensate for the low ionic conductivity of LSCF, a composite of LSCF with high ionic conductivity ceramic such as gadolinium doped ceria ($Gd_{0.1}Ce_{0.9}O_{1.95}$, GDC) is often employed. In this study, we report the development of a high surface area and highly porous LSCF-GDC composite cathode for IT-SOFC applications. The LSCF and GDC nanopowders were prepared via a solution combustion synthesis method. The nanocomposite cathode materials were prepared by mixing LSCF and GDC in 50:50 wt%. Symmetric cells were fabricated by depositing LSCF-GDC nanocomposite on GDC electrolyte at 130 °C via spray deposition method using an ultrasonic spray nozzle. The cells were sintered at 1000 °C and 1100 °C employing rapid microwave heating. To assess the effects of microwave sintering, LSCF-GDC samples were sintered with conventional resistance heating and compared with the microwave sintered samples. The morphology, microstructure, surface area, pore-volume, and pore size of the LSCF-GDC system were explored. To evaluate the electrical performance of the LSCF-GDC cathode, DC conductivity measurements were performed at the intermediate operating temperatures (500-800 °C).

Keywords: IT-SOFC, LSCF-GDC nanocomposite, Conventional Sintering, Microwave Sintering

Abbreviations

IT	Intermediate Temperature
SOFC	Solid Oxide Fuel Cell
EIS	Electrochemical Impedance Spectroscopy
PEMFC	Polymer Electrolyte Membrane Fuel Cell
AFC	Alkaline Fuel Cell
MCFC	Molten Carbonate Fuel Cell
PAFC	Phosphoric Acid Fuel Cell
TEC	Thermal expansion coefficient
ORR	Oxygen reduction reaction
OCV	Open-circuit voltage
CCL	current collector layer
CFL	Cathode functional layer
MIEC	Mixed ionic and electronic conduction
FIB-SEM	Focused ion beam scanning electron microscopy
NTs	Nanotubes
NPs	Nanoparticles
PVD	Physical Vapor Deposition
RF	Radiofrequency
SE	Secondary electrons
BSE	Backscattered electrons
CRT	cathode ray tube
EDS	Energy dispersive spectroscopy
XRD	X-ray diffraction
JCPDS	Joint Committee on Powder Diffraction Standards

CS   Conventionally sintered

MS   Microwave sintered

Chapter 1

Introduction

1.1 Background

Since the beginning of the time human strive for a better life in this regard made thousands of inventions, which changed the life of man. One of the biggest discoveries is electricity which changed the course of human history over time man invented many methods to generate electricity. For electricity generation, man harnessed the water resources, utilized fossil fuels, and oil. Electricity revolutionized the industry, over time as energy demand grew so did the pollution associated with resources that affected the environment. To address the environmental issues researchers and scientists worked on the resources with are environment friendly with the passage of the different alternate energy resources were developed which include wind, solar, geothermal, ocean energy, and fuel cells. A fuel cell is a device that converts chemical energy into electrical energy by harnessing the electrons exchanged during the chemical reaction of two species i.e. fuel and oxidant. Fuel cells are the environment-friendly mode for power generation and choice for zero-emission power sources. Its advanced energy generation technology for the future. Earlier man relied on fossil fuel resources for power generation which resulted in pollution due to the emission of SO_x, NO_x, and CO from fossil fuel burning as well as pollutant particulates which harm the environment and human life. With industrialization the power demand raised consequently, consumption of fossil fuel increased the pollution. Conventional power generation technologies are main causing global warming. As time passed, renewable energy resources evolved and countered the pollution problem to some extent but these technologies have their drawbacks. The intermittent nature of these resources requires storage systems. However, these technologies are used for transportation except batteries and super capacitors. Nowadays hydrogen fuel is in limelight for usage in the transportation sector generated from renewable energy resources in combination with fuel cells used for efficient and clean means of energy conversion, and generating power. Fuel cells are can also be used for stationary applications from mobile phones, laptops to stand-alone power supply resources.

1.2 Fuel Cell

Fuel cells operate like batteries; they convert chemical energy into electrical energy but differ from batteries as long as fuel and oxidant are supplied. In the year 1839, William Grove performed the first demonstration of a fuel cell. It was operated on oxygen and hydrogen with platinum electrodes in the solution of sulfuric acid. Solid oxide fuel cells began in 1899 when Nernst demonstrated the first yttria-stabilized zirconia ionic conductor. In the decade 1960 the first fuel cell for practical applications and used in the US for Gemini and Apollo space programs. Since then research started for its commercialization for instance in 1993 Ballard Power showed the first fuel cell-powered bus. After that, many competitors developed vehicles powered by fuel cells in Japan, the USA, and Europe. For stationary applications, hundreds of systems are installed around the globe. In the year 2005, Samsung demonstrated a portable application, a fuel cell-powered laptop that worked for 15 hours. However, the most significant obstacle is cost reduction for its practical application on large scale. The increasing focus on fuel cell commercialization is due to several advantages. These advantages are clean energy because the by-product of fuel cells operated on hydrogen is water and extremely low emissions. Furthermore, they have high power density and high efficiency of up to 40%, the waste heat from the fuel cell can be used for combined heat and power generation which improves its overall. Many types of fuel cells operate on a wide range of fuels like methanol, ethanol, H_2, natural gas [33].

1.2.1 Working

A fuel cell reaction occurs between fuel and oxidant at the electrode-electrolyte interface. The electrode where fuel is supplied is called an anode and the electrode where an oxidant is supplied is called the cathode. In between both electrode, the electrolyte is sandwiched and ions from travels through the electrolyte and combined to form the product. In figure 1.1 a fuel cell is shown in which H_2 is used as fuel while O_2 is as oxidant. An O^{-2} is produced at the cathode, travels through the electrolyte, and combines with H_2 to form water as a product.

The following reactions take place at anode and cathode:

$$\text{Anode:} \quad H_2 + O^{-2} \rightarrow H_2O \ldots\ldots\ldots\ldots (1.1)$$

$$\text{Cathode:} \quad \frac{1}{2}O_2 + 2e^- \rightarrow O^{-2} \ldots\ldots\ldots (1.2)$$
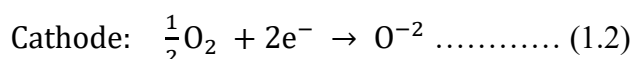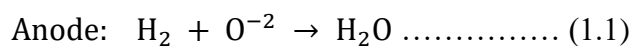
1.3 Fuel Cell Types

The fuel cell types are categorized based on the type of the fuel, electrolyte, and working temperature, which are:

- Solid Oxide Fuel Cell (SOFC)
- Polymer Electrolyte Membrane Fuel Cell (PEMFC)
- Alkaline Fuel Cell (AFC)
- Molten Carbonate Fuel Cell (MCFC)
- Phosphoric Acid Fuel Cell (PAFC)

Table 1.1: Types of fuel cell

	SOFC	MCFC	AFC	PAFC	PEMFC
Electrolyte	Ceramic	Molten Carbonate	KOH (liquid-Immobilized)	H_3PO_4 (Liquid)	Polymer Membrane
Electrodes	Ceramic	Ni	Pt	Graphite Electrodes	Porous Carbon
Operating Temperature	600-1000ºC	650ºC	60-250ºC	180-210ºC	90ºC
Charge Carrier	H^+	CO_3^{-2}	OH^-	H^+	H^+
Catalyst	Electrode as Catalyst	Electrode as Catalyst	Platinum	Platinum	Platinum
Fuel	H_2, CH_4,CO	H_2, CH_4	Hydrogen	Hydrogen	Hydrogen
Efficiency	50-60%	45-50%	50%	40%	30-40%
Advantage	Fuel Flexibility	Fuel Flexibility, High Quality Waste Heat	Low material and Electrolyte Cost	Mature Technology, Low Cost Electrolyte, Reliable	High Power Desnity, Portable Applications
Disadvantage	Degradation, Expensive Components, Long Startups	Corrosion, Degradation Issue	Pure H_2 - O_2 needed, KOH replenishment	Expensive Catalyst, CO & S poisoning	Expensive Catalyst, Expensive Ancillary Components

Solid oxide fuel cells have many advantages like combined heat and power generation its efficiency can reach up to 90%. Due to the disadvantage of the SOFC, it is facing many issues for commercialization like its lifetime and cost fabrication. The focus of this study is to explore materials for cathode, which can operate at intermediate temperature (500-800°C) solid oxide fuel cells [33].

1.4 Solid Oxide Fuel Cell (SOFC)

Solid oxide fuel cell is the focus of researchers due to its ability for combined heat and power generation, which increases its overall efficiency to 90%, with low emission of pollutants. The main issue for commercialization is its lifetime and cost of fabrication, which are associated with its operating temperature, which is up to 1000°C. The focus of this study is to explore materials for cathode, which can operate at a lower temperature (500-800°C).

1.4.1 SOFC Operation

The solid oxide fuel cell (SOFC) works similarly to another fuel cell. The oxidant e.g. oxygen is supplied at the cathode where oxygen reduction reaction occurs and O^{-2} travel through the ceramic electrolyte through electrolyte towards anode where hydrogen oxidation reaction (HOR) occurs and O^{-2} combines with H^{+} to form water a product of SOFC and electrons travels through current collectors towards load similar to as shown in figure 1.2.
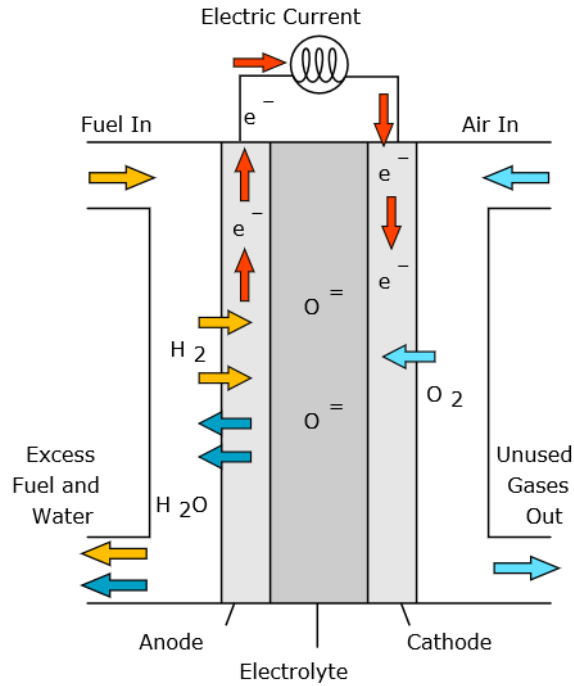
Figure 1.1: Soxide fuel cell working [36]

The following reactions take place at anode and cathode:

$$\text{Anode:} \quad H_2 + O^{-2} \rightarrow H_2O \quad \ldots\ldots\ldots\ldots\ldots(1.3)$$

$$\text{Cathode:} \quad \frac{1}{2}O_2 + 2e^- \rightarrow O^{-2} \quad \ldots\ldots\ldots\ldots\ldots(1.4)$$
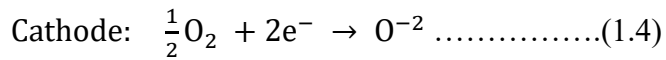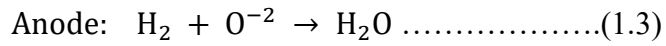
The steps involved in the power generation are

1) Reactant Delivery to fuel cell
1) Reactions at Anode and Cathode
2) Ionic and Electronic conduction through the electrolyte and External circuit respectively
3) Product removal
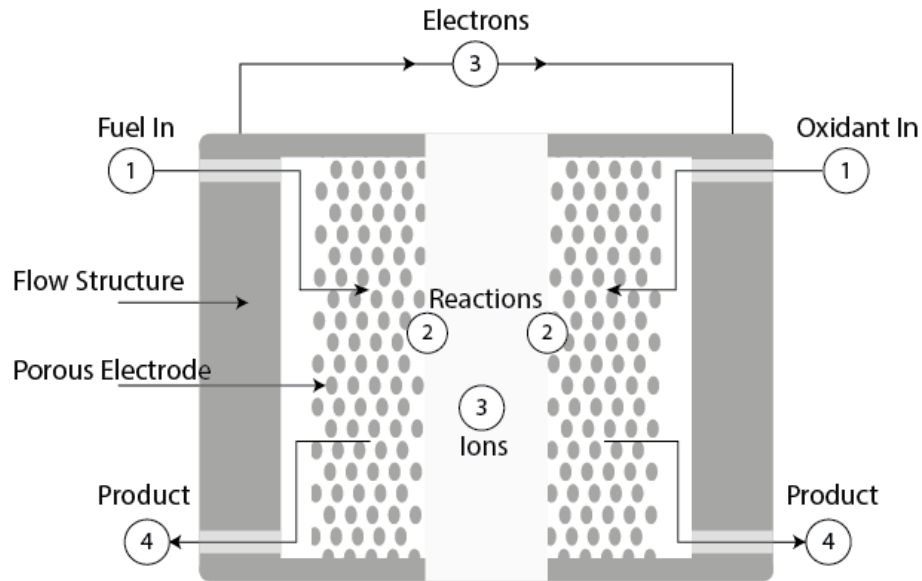
Figure 1.2: Fuel Cell Cross-section showing steps for power generation through an electrochemical reaction [34]

The first step in power generation is continuous fuel and oxidant supply. For high current, the reactants must be supplied quickly enough which is achieved by using flow plates with porous electrodes. The shape, size, and pattern of flow channels affect the fuel cell performance.

The second step is an electrochemical reaction; the power generated depends upon the speed of the electrochemical reaction. To achieve a high reaction rate high surface area electrode is used which provides the high catalytic activity.

The electrochemical reaction in fuel cell produces or consume ions and electrons. Ion and electrons are produced at one electrode and consumed at the other electrode. Electrons transfer through the wire between two electrodes. Similar holds for ions but ions are larger and heavier than the electrons, therefore; ions transport is difficult and less efficient and causes cell performance reduction. Therefore, electrolytes are made as thin as possible for efficient and easy ions transport.

The last step in the power generation cycle is product removal. Electrochemical reactions in fuel produce by-products like water and carbon dioxide, these products are removed to avoid choking off fuel cells [34].

1.4.2 Cell performance

The performance of the fuel cell is understood by the Current-Voltage curve as shown in figure 1.3. The current produced depends upon the area of the fuel cell; larger fuel can produce more power than a smaller area fuel cell. A fuel cell can provide any current as long as reactants are supplied.
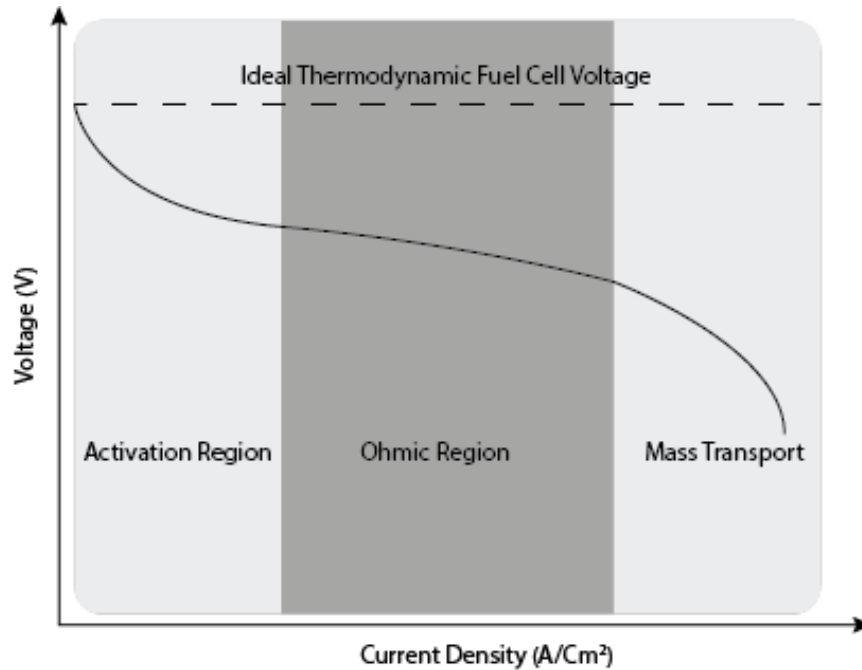
Figure 1.3: Current-voltage curve of fuel cell

The power produced by the fuel cell is determined using

$$P = iV \ \text{.............. (1.5)}$$

A power-density curve provides power density delivered as the current density function.

This curve is plotted by multiplying voltage at every point with a corresponding current density as shown in figure 1.4.
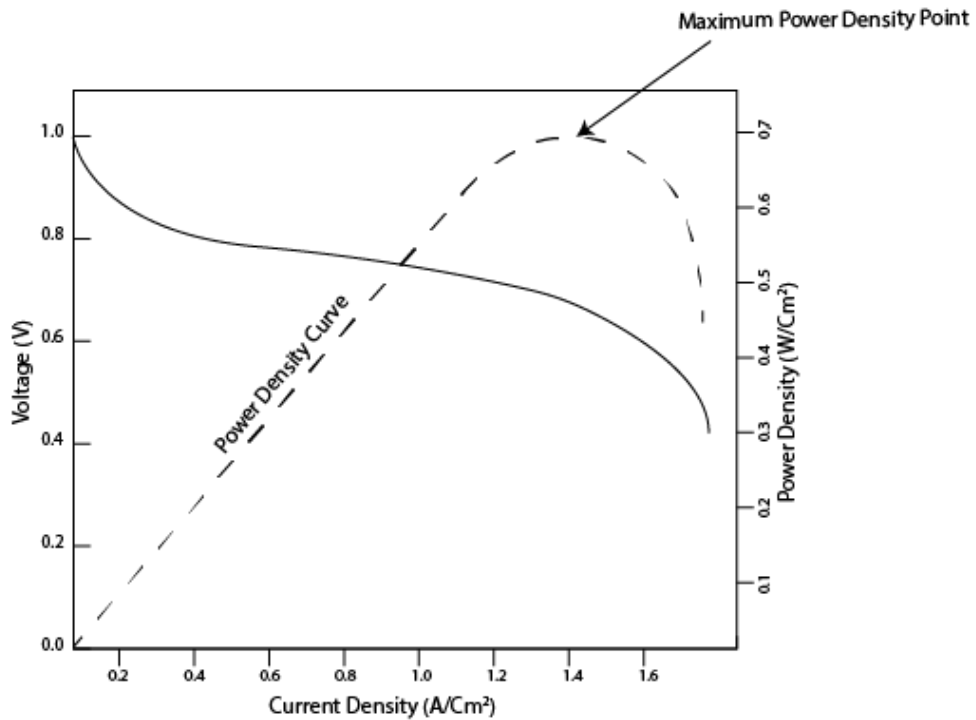
Figure 1.4 Power density curve of fuel cell[34]

Fuel cell power density tends to increase as current density increases, reaches the maximum, and falls. At current density below power, density is maximum voltage efficiency is increased but power falls. At current density above the maximum power density, both voltage, and power fall.

The voltage produced by the fuel cell is less than the thermodynamic voltage due to losses associated with the fuel cell,

1) Activation Losses caused during Electrochemical Reactions)
2) Ohmic losses (Ions and Electronics)
3) Concentration losses (associated with mass transport)

The fuel cell voltage is written by subtracting losses from output voltage, this is given by the following equation:

$$V = E_{thermo} - \eta_{act} - \eta_{ohnic} - \eta_{conc.} \quad \ldots\ldots\ldots\ldots(1.6)$$

"E" actual output voltage, "E_{thermo}" thermodynamically predicted output voltage, "η_{act}" activation losses (reaction kinetics), "η_{ohmic}" electronic & ionic losses, "η_{conc}" concentration losses (mass transport) [34].

1.4.3 Cell Components

The solid oxide fuel cell's main components are the anode, electrolyte, and cathode.

8

Solid oxide fuel cell is composed of solid materials; operate at higher temperature ($1000^{\circ}C$). The principal components of the fuel cell are Electrolyte, Anode, and Cathode. The electrodes in the fuel cell provide reactants and maintain contact between three-electrode, electrolyte, and gases. The anode role is to provide fuel over its whole surface and conduct electrons to an external circuit liberated from hydrogen. Cathode distributes oxygen and conducts electrons from the external circuit to combine with oxygen ions to form O_2 and form hydrogen to form water. The electrolyte and interconnects serve the purpose of avoiding the mixing of fuel and oxidant. The cell components should be chemically compatible with each other, have good stability in an oxidizing and reducing environment, have low cost, and similar thermal expansion coefficient (TEC).

1.4.3.1 Electrolyte

In the fuel cell, electrolyte material is of great importance, it blocks the electrons and allows the ions to pass and avoid the fuel and oxidant mixing. Many electrolyte materials are employed in intermediate-temperature solid oxide fuel cells. For instance, ZrO_2 electrolyte with high stability but low conductivity, on the other hand, Bi_2O_3-based electrolyte have poor stability but high ionic conduction [1]
. Doped CeO_2 is suitable for $450–600^{\circ}C$ but limited application due to internal current. Whilst proton conducting material due to low activation energy are suitable for intermediate temperatures. Mainly proton conducting materials are perovskite-based structures. However, these materials lack high conductivity and chemical stability in SOFC operating conditions e.g. oxidizing and reducing environments. In general, $BaCeO_3$-based possess poor chemical stability but good conductivity, while $BaZrO_3$ electrolytes are vice versa. A combination of both to produce a new $BaCe_xZr_{1-x}O_3$ electrolyte is a good option e.g. BCZY712 is widely researched. One kind of dual conducting is a mixture of doped CeO_2 and carbonate composites, such as SDC/Na_2CO_3. While keeping in mind the requirements of electrolyte materials such as chemical and mechanical stability and ionic conductivity the electrolyte can perform well. Coating doped ceria on zirconia avoids chemical reactions between electrolyte and cathode materials such as BCSF & LSCF. A doped-ceria electrolyte layered with LSGM not only avoids reaction between electrode and LSGM but also provides high open-circuit voltage. ZrO_2 and δ-Bi_2O_3 combined provides mechanical strength and

9

chemical stability thus promoting oxygen reduction reaction (ORR). A layer of doped ceria between δ-Bi_2O_3 and anode avoids reduction of δ-Bi_2O_3 and blocks electronic conduction [2]. Co-doped ceria electrolyte with ytterbium and samarium $(Ce_{1-y}Sm_xYb_yO_2$ y=x=0.05-.01) were prepared by the sol-gel method. The co-doping enhanced ionic conduction by improving morphology, electrical properties, and structure.

The composition of $Ce_{0.85}Sm_{0.1}Yb_{0.05}O_{1.925}$ showed lowest value of activation energy f 0.63eV and hight ionic conductivity value of $7x10^{-3}$ S/cm at 500^oC [3].Two Sm co-doped systems with $Ce_{0.8}Gd_{0.2}O_2$ were developed by auto-combustion synthesis as $Ce_{0.9-x}Sm_xGd_{0.1}O_2$ and $Ce_{0.9}Sm_xGd_{0.1-x}O_2$ (x=0-0.1) and structural impact of Sm was observed. Oxygen vacancy concentration was found to be highest for 10%,10% Sm and Gd, Ce co-doped ceria electrolyte ($Ce_{0.8}Sm_{0.1}Gd_{0.1}O_{1.90}$) which is $2.65x10^{-23}cm^{-3}$ with Raman Spectroscopy. Impedance spectroscopy revealed improved Ionic conduction $0.147x10^{-3}$S/cm for $Ce_{0.8}Sm_{0.1}Gd_{0.1}O_{1.90}$ and activation energy of 0.85eV [4]. A $Sm_{0.2}Ce_{0.8}O_2$ (SDC) composite with co-doped barium cerate ($BaZr_{0.1}Ce_{0.7}Y_{0.1}Yb_{0.1}O_3$) was developed by mechanically mixing both with 10% and 30% BZCYYb.

SDC with 15% BZCYYb showed the lowest value of resistance $0.641\Omega cm^2$ and power density of 0.56W/cm at 600^oC due to increased boundary conduction and excellent compatibility between two materials. The conduction results for 15B85S and 30B70S were 0.013S/cm and 0.017S/cm at 600^oC [5]. Indium doped in $Nd_2Ce_2O_7$ ($Nd_{2-x}In_xCe_2O_7$, x=0-0.20) electrolyte developed by sol-gel method. Dopant improved structural, electrical properties and increased the grain growth of NdCeO electrolytes. The $Nd_{1.85}In_{0.15}Ce_2O_7$ composition of electrolyte exhibited conductivities of $0.75x10^{-2}$S/cm in air and $2.07x10^{-2}$ S/cm in H_2. In single-cell conditions,s the power density of $743mW/cm^2$ at 700^oC was achieved [6]. A ceria (CeO_2) co-doped with scandia (Sc_2O_3) and Samaria (Sm_2O_3) was prepared with $Sc_xSm_{0.2-x}Ce_{0.8}O_{1.9}$ (SSDCX) (x=0-0.08). The results showed the co-doping of ceria performed well than only Samaria doping, co-doping suppressed ceria reduction which improved the chemical stability of electrolytes. The power density value of 0.225 W/cm^2, electrical conductivity of $2.64x10^{-2}$S/cm, and 0.87V open-circuit voltage (OCV) at 700^oC was recorded for $Sc_{0.04}Sm_{0.16}Ce_{0.8}O_{1.9}$ [7].

1.4.3.2 Anode

One important component of the fuel cell is the anode, which acts as a catalyst for fuel and provides electron current to an external load. The desired properties of an anode are high electrical conductivity, thermal coefficient match (TEC), porous, good ionic and electronic conduction, chemical and mechanical stability. Ni−YSZ cermets is a good anode for H_2 conversion but highly depends on microstructure, porosity, and particles size. Lanthanides containing materials displayed a wide range of physical properties. demonstrated that several perovskites such as $LaCrO_3$, and $SrTiO_3$ [8]. Perovskite material has also been the ceramic material of choice to be used with Ni namely such as zirconium & yttrium doped barium CeO_2 (BZCY) and lanthanum doped strontium titanate (LST) displayed power density higher than 0.225 W/cm2 [9]. $Gd_{0.1}Ce_{0.9}O_2$ - $Sr_2 Fe_{1.3}Co_{0.2}Mo_{0.5}O_6$ (SFCM-GDC) resulted a power density of 0.986 W/cm^2 and R_p of 0.35 Ω cm^2 at 800ºC [10]. Ni and YSZ with ceramic Ag showed power density of 0.463 and 0.251 W/cm^2 for Hydrogen and methane respectively [11].

For increasing the mechanical strength of the anode material is has been shown that a mix of YSZ, NiO, and copper at low sintering temperature produces high strength and good porosity [12]. Another anode nickel-samarium doped ceria (Ni-SDC) showed maximum power densities 239-270 mW/cm^2 at 600-700ºC [13]. Ni and $BaZr_{0.4}Ce_{0.4}Y_{0.2}O_{3-\delta}$ (Ni-BZCY) anode exhibit good electrochemical stability and coking resistance, in addition, Ni-BZCYYb resulted in a peak power density of 900mW/cm^2 at 750ºC using ethanol fuel [14]. Nano-sized Lanthanum doped Strontium titanate ($SrTiO_3$) composite cathode with Samaria-doped ceria (SDC) both prepare by glycine nitrate method, and deposited onto $La_{0.8}Sr_{0.2}Ga_{0.8}Mg_{0.2}O_3$ (LSGM) electrolyte exhibited 40% porosity with fine structure enhanced the triple-phase boundary, and gas permeability which increased the performance of fuel cell. When anode was annealed at 1250 ºC for 5 h, the power density of the cell increased to 301 mW/cm^2 from 221mW/cm^2 (as-sprayed) at 800ºC[15]. Ferrite-based $La_{0.5}Sr_{0.5}Fe_{0.9}Mo_{0.1}O_3$ (LSFMo) anode was developed. A Samaria doped ceria (SDC) interlayer was introduced between the electrode (LSFMo) and electrolyte (LSGM) this resulted in polarization resistance reduced and its values were 1.54, 0.83, 0.50, and 0.33 Ωcm^2 at 700, 750, 800, and 850ºC in H_2, respectively. In single configuration

power densities and resistance were 1078 mW/cm^2 and 0.29 Ωcm^2 for hydrogen and 769 mW/cm^2 and 0.39 Ωcm^2 for methane at 850°C[16]. Cobalt-based Pr$_{0.5}$Ba$_{0.5}$Co$_{0.25}$Fe$_{0.75}$O$_3$ perovskite anode material composite with gadolinium-doped ceria exhibited low 0.05 Ωcm^2 and 0.21 Ωcm^2 in air and in H$_2$ at 700°C. Due to a good oxygen reduction reaction, the catalytic activity of ceramic in composite symmetric cells showed a power density of 0.75W/cm^2 at 750°C[17]. A novel Co-based Sr$_{1.95}$Fe$_{1.4}$Co$_{0.1}$Mo$_{0.5}$O$_6$ (SFCoMo) anode was prepared, which possessed high catalytic activity and carbon tolerance. The cell performance test showed a power density of 0.79 for C$_3$H$_8$ and 1.01for H$_2$ at 750°C[18].

1.4.3.3 Cathode

Like all other types of fuel cell cathode is a major component of the intermediate temperature solid oxide fuel cell and extensive research is going on to optimize the cathode material to achieve properties desired in an ideal fuel cell material for instance chemical stability, high oxygen reduction activity, mechanical stability, and porosity. A cobalt-free Niobium based perovskite cathode Bi$_{0.5}$Sr$_{0.5}$Fe$_{1-x}$Nb$_x$O$_3$ (X= 0.05, 0.1., 0.15) Developed showed polarization resistance of 0.038, 0.075 and 0.156 Ω/cm^{-2} at 700, 650 and 600 °C, respectively. In single-cell configuration exhibited power densities of 1.28, 1.54, and 1.34 W cm$_{-2}$ at 700 °C [19]. Another cobalt-free cathode anode is La$_{0.8}$Sr$_{0.2}$Zn$_x$Fe$_{1-x}$O$_3$ (LSZF, x= 0.1, 0.2, 0.3).

The anode was deposited onto samarium doped ceria (SDC) with x=0.2 resulted in remarkable cell performance such as thermal stability 12.10µ/K, the electrical conductivity of = 13.63 S/cm, and low specific resistance = 0.69 Ωcm^2. A power density of 409mW/cm^2 was recorded at 550°C [20]. A layered perovskite anode material PrBa$_{0.92}$CoCuO$_6$ was prepared with Cu^{+2} doping at b-site in parent PrBaCo$_2$O$_6$ with high oxygen vacancies showed electrical conductivity of 134 S/cm and 22 S/cm at 800 and 400°C in air. The fuel cell performance was improved as specific resistance of 0.12 and 0.017 Ωcm^2 at 600 and 750°C respectively, and 25% less TEC than the parent material. In single-cell arrangement the values of power densities were 1541, 1228, 930 mW/cm^2 at 800, 750 and 700°C respectively [21].

LaBa$_{0.5}$Sr$_{05}$Ca$_{025}$Co$_2$O$_5$ (LBSCaCoO) was investigated along with Ca-free same material. The TEC of Ca doped cathode material was reduced from 26x10^{-6}/K to 20x10^{-6}/K. The electric conduction value of the doped material was 500 S/cm. The

electrochemical results showed resistance values of 0.084 Ωcm^2 for LBSCo and 0.075Ωcm^2 for LBSCaCo at 800°C. For Ca doped LBSCo the power density of 662mW/cm^2 at 800°C [22]. A LaCoO coated BSCF cathode material prepared by solution impregnation method was investigated for polarization and Co poisoning resistance. After coating cathode showed a resistance value of 0.197 Ωcm^2 and 0.243W/cm^2 power density at 600°C and excellent CO_2 resistance as compared to bear BSCF cathode [23]. A Ca-doped double-layered perovskite $NdBa_{1-x}Ca_xCoCuO$ (x=0, 0.3) synthesised employing sol-gel method. Doping of Ca enhanced electrical and chemical compatibility. The power densities recorded were 1.42W/cm^2 and 1.84 for x=0 and x=0.3 respectively at 800°C [24].

LSCF The polarization resistance of LSCF is 0.272Ωcm^2 at 600°C, 0.116 Ωcm^2 at 650°C, 0.063 Ωcm^2 at 700°C, 0.039 Ωcm^2 at 750°C, and 0.029 Ω/cm^2 at 850°C a perovskite material cathode was synthesized using glycine nitrate process [25]. In another study, a 200nm-CGO layer was introduced between LSCF cathode and YSZ electrolyte to avoid the formation of $La_2Zr_2O_7$ and $SrZrO_3$ which increase the cell resistance. After introducing CGO layer polarization resistance reduced from 47.7Ωcm^2 to 7Ωcm^2 at 800°C [26]. $La_{0.4}Sr_{0.6}Co_{0.2}Fe_{0.8}O_3/Ce_{0.9}Gd_{0.1}O_2$ composite cathode was prepared from LSCF-GDC powder synthesized by ball milling the precursors and screen printing them onto electrolyte. The nanoparticles showed low polarization resistances of 0.69 Ωcm^2 at 650°C, 0.38Ωcm^2 at 700°C, 0.17Ωcm^2 at 750°C, and 0.08Ωcm^2 at 800°C [27].

In another study, CGO barrier layers were introduced between LSCF cathode and YSZ electrolyte. In one method CGO was deposited by airbrushing and in the second method LSCF was deposited by spray pyrolysis on dense CGO which resulted in low fabrication temperature and Sr surface enrichment avoided at intermediate temperature (650°C) [28]. An $La_{0.6}Sr_{0.4}Co_{1-y}Fe_y$ perovskite cathode was fabricated by electrospinning for y=0.2,0.4,0.6,9.8,1.0. The results indicated that as the Fe content increased polarization resistance decreased as temperature increased [29].

An LSCF-GDC composite cathode was fabricated electrostatic spray deposition. When LSCF was used as the current collector layer (CCL), resulted in an R_p=1.3Ωcm^2 decrease of 1.5 orders of magnitude compared to a single cathode functional layer (CFL) without and current collector layer at 600°C [30]. LSCF-GDC composite cathode was fabricated which was infiltrated with CuO particles redox reaction at interface caused to decrease specific resistance. A decrease in specific resistance from

15.5 to 3.9 Ωcm^2 and 0.62 to 0.32 Ωcm^2 was observed at 500 and 650°C respectively [31]. $La_{0.4}Sr_{0.6}$ $Co_{0.2}Fe_{0.8}O_3/Ce_{0.8}Gd_{0.2}O_2$ composite cathode deposited onto electrolyte by plasma spray technique with GDC content in solution of 0 to 15 g/L, LSCF-GDC composite porous cathode (~40%) indicated better results than blank LSCF cathodes. The cathode with 15g/L GDC content resulted in better specific area resistance which is 0.009 Ωcm^2 and 0.1 Ωcm^2 at 750 and 650°C respectively [32] $La_{0.4}Sr_{0.6}Co_{0.2}Fe_{0.8}O_3/Ce_{0.9}Gd_{0.1}O_2$ nanocomposite cathode was prepared to employ spray deposition pyrolysis with LSCF varying content from (50-100%). CGO addition limits the grain growth, which in turn improved resistance values 0.30 for 100%LSCF and 0.15 for 50%LSCF at 600°C. Power density improved from 0.56 W/cm^2 screen-printed cathode to 0.90 W/cm^2 for spray pyrolysis deposition at 600°C [33].

1.4   Current Challenges in SOFC

The solid oxide fuel cells operate at a high temperature of 800°C to 1000°C and are given good overall performance when used in combined heat and power generation. However, there are some difficulties associated with the high-temperature operation, like the cost of materials e.g. ceramic materials used for its fabrication, which will eventually increase its cost, which is a hurdle in its commercialization. The high temperature and long hours associated with materials sintering for cell fabrication deteriorate the porous structure of the material reducing its catalytic activity. The temperature operation reduces SOFC fuel cell performance over time due to material degradation, the long startup and showdown duration is an obstacle for portable applications. The development of material used for reduced operating temperature 600-800°C is an important research focus.

Summary

Fuel cells are chemical devices, which convert the chemical energy of fuels to electrical energy. In many types of fuel cells, solid oxide fuel cells (SOFC) are most efficient because they offer an advantage of combined heat and power generation and o board hydrocarbon reforming, and a wide range of fuel. SOFC operates between 800-1000°C called high temperatures SOFC. The basic components of this fuel cell are similar to any anode, a cathode, and an electrolyte. The current challenge associated with SOFC is to reduce its high temperature to make it cost-efficient for commercialization and increase its durability. In this context, materials are developed to operate SOFC between 500-800°C an intermediate temperature solid oxide fuel cell (IT-SOFC). In this regard many types of cathodes materials are used in IT-SOFC, LSCF is a promising cathode material because it exhibits electronic as well as ionic conductions and is called mixed ionic and electronic conductors (MIEC). There will be a detailed discussion on LSCF based cathode materials for IT-SOFC.

References

[1]   N. Mahato, A. Banerjee, A. Gupta, S. Omar, and K. Balani, "Progress in material selection for solid oxide fuel cell technology: A review," *Prog. Mater. Sci.*, vol. 72, pp. 141–337, 2015, doi: 10.1016/j.pmatsci.2015.01.001.

[2]   H. Shi, C. Su, R. Ran, J. Cao, and Z. Shao, "Electrolyte materials for intermediate-temperature solid oxide fuel cells," *Prog. Nat. Sci. Mater. Int.*, vol. 30, no. 6, pp. 764–774, 2020, doi: 10.1016/j.pnsc.2020.09.003.

[3]   L. A. Eressa and P. B. Rao, "Synthesis and characterization of Ytterbium and Samarium Co-doped ceria as an electrolyte for intermediate-temperature solid oxide fuel cell application," *Mater. Chem. Phys.*, vol. 242, no. July 2019, p. 121914, 2020, doi: 10.1016/j.matchemphys.2019.121914.

[4]   S. Ajith Kumar, P. Kuppusami, S. Amirthapandian, and Y. P. Fu, "Effect of Sm co-doping on structural, mechanical and electrical properties of Gd doped ceria solid electrolytes for intermediate temperature solid oxide fuel cells," *Int. J. Hydrogen Energy*, vol. 45, no. 54, pp. 29690–29704, 2020, doi: 10.1016/j.ijhydene.2019.10.098.

[5]   M. Xia *et al.*, "Effects of co-doped barium cerate additive on morphology, conductivity and electrochemical properties of samarium doped ceria electrolyte for intermediate temperature solid oxide fuel cells," *Int. J. Hydrogen Energy*, vol. 43, no. 33, pp. 16293–16301, 2018, doi: 10.1016/j.ijhydene.2018.07.040.

[6]   B. Zhang, K. Wu, and K. Peng, "Fabrication and characterization of Nd2-xInxCe2O7 proton-conducting electrolytes for intermediate-temperature solid oxide fuel cells," *J. Power Sources*, vol. 399, no. May, pp. 157–165, 2018, doi: 10.1016/j.jpowsour.2018.07.073.

[7]   Y. Gan, J. Cheng, M. Li, H. Zhan, and W. Sun, "Enhanced ceria based electrolytes by codoping samaria and scandia for intermediate temperature solid oxide fuel cells," *Mater. Chem. Phys.*, vol. 163, pp. 279–285, 2015, doi: 10.1016/j.matchemphys.2015.07.041.

[8]   S. P. S. Shaikh, A. Muchtar, and M. R. Somalu, "A review on the selection of anode materials for solid-oxide fuel cells," *Renew. Sustain. Energy Rev.*, vol. 51, pp. 1–8, 2015, doi: 10.1016/j.rser.2015.05.069.

[9]   S. Kim, C. Kim, J. H. Lee, J. Shin, T. H. Lim, and G. Kim, "Tailoring Ni-based catalyst by alloying with transition metals (M = Ni, Co, Cu, and Fe) for direct hydrocarbon utilization of energy conversion devices.," *Electrochim. Acta*, vol. 225, pp. 399–406, 2017, doi: 10.1016/j.electacta.2016.12.178.

[10]   Y. Yang *et al.*, " One Step Synthesis of $Sr_{0.2}Fe_{1.3}Co_{0.2}Mo_{0.5}O_{6-\delta}$ - $Gd_{0.1}Ce_{0.9}O_{2-\delta}$ for Symmetrical Solid Oxide Fuel Cells ," *J. Electrochem. Soc.*, vol. 167, no. 8, p. 084503, 2020, doi: 10.1149/1945-7111/ab8927.

[11]   X. Wu *et al.*, "Enhanced electrochemical performance and carbon anti-coking ability of solid oxide fuel cells with silver modified nickel-yttrium stabilized zirconia anode by electroless plating," *J. Power Sources*, vol. 301, pp. 143–150, 2016, doi: 10.1016/j.jpowsour.2015.10.006.

[12]   Y. Li *et al.*, "Achieving high mechanical-strength CH_4-based SOFCs by low-temperature sintering (1100 °C)," *Int. J. Hydrogen Energy*, vol. 45, no. 4, pp. 3086–3093, 2020, doi: 10.1016/j.ijhydene.2019.11.100.

[13]   A. Ideris, E. Croiset, and M. Pritzker, "Ni-samaria-doped ceria (Ni-SDC) anode-supported solid oxide fuel cell (SOFC) operating with CO," *Int. J. Hydrogen Energy*, vol. 42, no. 14, pp. 9180–9187, 2017, doi: 10.1016/j.ijhydene.2016.05.203.

[14]   W. Wang, Y. Chen, F. Wang, M. O. Tade, and Z. Shao, "Enhanced electrochemical performance , water storage capability for solid oxide fuel cells operating on ethanol," *Chem. Eng. Sci.*, vol. 126, pp. 22–31, 2015, doi: 10.1016/j.ces.2014.12.011.

[15]   S. L. Zhang, C. X. Li, and C. J. Li, "Chemical compatibility and properties of suspension plasma-sprayed SrTiO3-based anodes for intermediate-temperature solid oxide fuel cells," *J. Power Sources*, vol. 264, pp. 195–205, 2014, doi: 10.1016/j.jpowsour.2014.04.094.

[16]   F.   Liu   *et   al.*,   "High   performance   ferrite–based   anode La0.5Sr0.5Fe0.9Mo0.1O3–δ for intermediate–temperature solid oxide fuel cell," *Electrochim. Acta*, vol. 255, pp. 118–126, 2017, doi: 10.1016/j.electacta.2017.09.157.

[17]   Y. Tao, Y. Zhou, W. Li, J. Shao, L. Bai, and X. Liu, "Intermediate-temperature solid oxide fuel cells with high performance cobalt-doped Pr0.5Ba0.5FeO3-δ anodes," *J. Alloys Compd.*, vol. 741, pp. 1091–1097, 2018, doi: 10.1016/j.jallcom.2018.01.167.

[18]   C. Xu *et al.*, "A highly active and carbon-tolerant anode decorated with in situ grown cobalt nano-catalyst for intermediate-temperature solid oxide fuel cells," *Appl. Catal. B Environ.*, vol. 282, no. September 2020, p. 119553, 2021, doi: 10.1016/j.apcatb.2020.119553.

[19]   L. Gao *et al.*, "A novel family of Nb-doped Bi0.5Sr0.5FeO3-Δ perovskite as cathode material for intermediate-temperature solid oxide fuel cells," *J. Power Sources*, vol. 371, no. May, pp. 86–95, 2017, doi: 10.1016/j.jpowsour.2017.10.036.

[20]   M. S. Javed, N. Shaheen, A. Idrees, C. Hu, and R. Raza, "Electrochemical investigations of cobalt-free perovskite cathode material for intermediate temperature solid oxide fuel cell," *Int. J. Hydrogen Energy*, vol. 42, no. 15, pp. 10416–10422, 2017, doi: 10.1016/j.ijhydene.2017.02.045.

[21]   X. Jiang *et al.*, "Characterization of PrBa0.92CoCuO6−Δ as a potential cathode material of intermediate-temperature solid oxide fuel cell," *Int. J. Hydrogen Energy*, vol. 42, no. 9, pp. 6281–6289, 2017, doi: 10.1016/j.ijhydene.2016.12.076.

[22]   C.   Yao   *et   al.*,   "Characterization   of   layered   double   perovskite LaBa0.5Sr0.25Ca0.25Co2O5+δ as cathode material for intermediate-temperature solid oxide fuel cells," *J. Solid State Chem.*, vol. 265, no. February, pp. 72–78, 2018, doi: 10.1016/j.jssc.2018.05.028.

[23]   P. Qiu *et al.*, "LaCoO3-Δ-coated Ba0.5Sr0.5Co0.8Fe0.2O3-Δ: A promising cathode material with remarkable performance and CO2 resistance for intermediate temperature solid oxide fuel cells," *Int. J. Hydrogen Energy*, vol. 43, no. 45, pp. 20696–20703, 2018, doi: 10.1016/j.ijhydene.2018.09.154.

[24] S. Pang *et al.*, "Enhanced electrochemical performance of Ca-doped NdBa1-xCaxCoCuO5+δ as cathode material for intermediate-temperature solid oxide fuel cells," *Ceram. Int.*, vol. 44, no. 17, pp. 21902–21907, 2018, doi: 10.1016/j.ceramint.2018.08.301.

[25] S. A. Muhammed Ali, M. Anwar, N. A. Baharuddin, M. R. Somalu, and A. Muchtar, "Enhanced electrochemical performance of LSCF cathode through selection of optimum fabrication parameters," *J. Solid State Electrochem.*, vol. 22, no. 1, pp. 263–273, 2018, doi: 10.1007/s10008-017-3754-5.

[26] D. Szymczewska, J. Karczewski, A. Chrzan, and P. Jasinski, "CGO as a barrier layer between LSCF electrodes and YSZ electrolyte fabricated by spray pyrolysis for solid oxide fuel cells," *Solid State Ionics*, vol. 302, pp. 113–117, 2017, doi: 10.1016/j.ssi.2016.11.008.

[27] X. Xi, A. Kondo, T. Kozawa, and M. Naito, "LSCF-GDC composite particles for solid oxide fuel cells cathodes prepared by facile mechanical method," *Adv. Powder Technol.*, vol. 27, no. 2, pp. 646–651, 2016, doi: 10.1016/j.apt.2016.02.022.

[28] L. dos Santos-Gómez, J. Hurtado, J. M. Porras-Vázquez, E. R. Losilla, and D. Marrero-López, "Durability and performance of CGO barriers and LSCF cathode deposited by spray-pyrolysis," *J. Eur. Ceram. Soc.*, vol. 38, no. 10, pp. 3518–3526, 2018, doi: 10.1016/j.jeurceramsoc.2018.03.024.

[29] M. Lubini *et al.*, "Electrochemical characteristics of La0.6Sr0.4Co1−yFeyO3 (y=0.2–1.0) fiber cathodes," *Ceram. Int.*, vol. 43, no. 12, pp. 8715–8720, 2017, doi: 10.1016/j.ceramint.2017.04.002.

[30] J. Sar, L. Dessemond, and E. Djurado, "Electrochemical properties of graded and homogeneous Ce0.9Gd0.1O2−δ–La0.6Sr0.4Co0.2Fe0.8O3−δ composite electrodes for intermediate-temperature solid oxide fuel cells," *Int. J. Hydrogen Energy*, vol. 41, no. 38, pp. 17037–17043, 2016, doi: 10.1016/j.ijhydene.2016.07.236.

[31] C. Gao, Y. Liu, K. Xi, S. Jiao, R. I. Tomov, and R. V. Kumar, "Improve the catalytic property of La0.6Sr0.4Co0.2Fe0.8O3/Ce0.9Gd0.1O2 (LSCF/CGO) cathodes

with CuO nanoparticles infiltration," *Electrochim. Acta*, vol. 246, pp. 148–155, 2017, doi: 10.1016/j.electacta.2017.05.138.

[32]   S. L. Zhang, C. J. Li, C. X. Li, G. J. Yang, K. Huang, and M. Liu, "Liquid plasma sprayed nano-network La0.4Sr0.6Co0.2Fe0.8O3/Ce0.8Gd0.2O2 composite as a high-performance cathode for intermediate-temperature solid oxide fuel cells," *J. Power Sources*, vol. 327, pp. 622–628, 2016, doi: 10.1016/j.jpowsour.2016.07.108.

[33]   L. dos Santos-Gómez, J. M. Porras-Vázquez, E. R. Losilla, F. Martín, J. R. Ramos-Barrado, and D. Marrero-López, "LSCF-CGO nanocomposite cathodes deposited in a single step by spray-pyrolysis," *J. Eur. Ceram. Soc.*, vol. 38, no. 4, pp. 1647–1653, 2018, doi: 10.1016/j.jeurceramsoc.2017.10.010.

[34]   M. M. Mench, *Fuel Cell Engines*. 1967.

[35]   R. O'HAYRE, *Fuel cell fundamentals*, Third. Wiley & Sons.

[36]   https://en.wikipedia.org/wiki/Solid_oxide_fuel_cell

Chapter 2

Solid Oxide Fuel Cell Cathode Materials

2.1 Lanthanum Strontium Maganese Cathodes

Lanthanum Strontium Manganese (LSM) systems with A-site substitution prove to have more cation vacancies which affect the electrical and electronic properties of the cathode. A copper-doped LSM material was developed through the EDTA-citrate method. $La_{0.8}Sr_{0.2}Mn_{1-x}Cu_xO_3$ showed highest electrical conduction 190 S/cm and low specific resistance of $4.3\Omega cm^2$ at 750^oC (x=0.2) as compared to blank LSM. This enhancement is owed to Mn^{+4} conversion to Mn^{+3} promoting oxygen vacancies [1]. An LSM-YSZ composite prepared through aerosol deposition process exhibited the area-specific resistance of 1.5 Ωcm^2 and power density of 0.38 mW/cm^{-2} at 800^oC. This performance is due to the electrocatalytic properties of materials and techniques used to deposit the electrode caused a strong connection between particles and layers due to high impact compressed air used for cathode fabrication of on YSZ electrolyte [2]. In another study, the cathodes LSM, LSM-YSZ, and LSM-YSZ-LSM were prepared to employ dip coating on YSZ electrolytes. The electrical conductivities 1.8-5.5 $x10^3$ S/m for LSM, 0.32-209 S/m for LSM-YSZ, $1.3-5.5x10^3$ S/m for LSM-YSZ-LSM between $1000-1200^oC$. And their activation energy values were found from conductivities as follows 0.104-0.146 eV for LSM-YSZ-LSM, 0.83-0.94 eV for LSM-YSZ, 0.106-0.147 eV for LSM. The YSZ present in LSM-YSZ composite and LSM-YSZ-LSM controlled the electrical conductivities [3]. Another study demonstrated the reduction in area-specific resistance (ASR) of ESB infiltrated with LSM. $Er_{0.4}Bi_{0.6}O_3$ (EBO) ink was deposited on GDC electrolyte and LSM was infiltrated with different concentrations of LSM solution (0.3-0.8M) and 0.5M LSM solution exhibited the lowest resistance $0.16\Omega cm^2$ 650^oC. The solid loading of infiltration precursor affected the electrochemical performance by improving the triple-phase boundary (TPB) and oxygen reduction reaction (ORR) due to the high porosity achieved by 0.5M solution [4]. Symmetrical cell performance was evaluated for $La_{0.5}Sr_{1.5}MnO_4$ (L5S15M) in Au/LSM/GDC/YSZ/GDC/LSM/Au configuration. The electrons transfer between

electrodes and oxygen, oxygen ions inclusion in electrodes, and oxygen reduction reaction (ORR) controlled the oxygen reduction reaction. A study showed as the sintering temperature of electrodes increased from 1150-1250°C the Sr surface enrichment increased at GDC/YSZ which increased the ASR of the symmetrical cell. The ASR values were taken at 800°C which are 1.32 Ωcm^2 sintered at 1150°C, 1.89 Ωcm^2 sintered at 1200°C, 73.44 Ωcm^2 sintered at 1250°C [5]. Phase segregation in any electrode causes a detrimental effect on fuel cell performance. In this study, Mn segregation from $La_{0.8}Sr_{0.2}MnO_3$ (LSM) was studied with 8% Y_2O_3 doped ZrO_3 and $Gd_{0.1}Ce_{0.9}O_{1.95}$ electrolyte. The LSM was screen printed on the electrolyte; interface and Mn segregation were studied performed using focused ion beam scanning electron microscopy (FIB-SEM). The result indicated the low ohmic resistance for both LSM-GDC and LSM-YSZ arrangements. However, in the case of LSM and YSZ, the LSM started to disintegrate and Mn segregated while for GDC it was relatively stable. This was due to localized heat generation at the electrode/electrolyte interface caused by low ionic conduction. But it did not cause a profound impact on fuel cell performance [6].

2.2 Barium Strontium Cobalt Ferrite Cathodes

$Ba_{1-y}Sr_yCo_{1-x}Fe_xO_3$ is a cubic perovskite material for solid oxide fuel applications. $Ba_{0.5}Sr_{0.5}Co_{0.8}Fe_{0.2}O_3$ (BSCF) powdered was prepared by citrate method and screen-printed on $Gd_{0.1}Ce_{0.9}O_{1.95}$. The powder was sintered 800-950°C in an air and nitrogen environment resulted in different microstructures, which influenced the electrochemical performance of the cell. The powder sintered in nitrogen environment exhibited the ASR of 0.78 Ωcm^2 at 500°C, 0.10Ωcm^2 at 600°C, 0.018 Ωcm^2 at 700°C, sintered at 900°C [7]. For improving the catalytic property of $Ba_{0.5}Sr_{0.5}Co_{0.8}Fe_{0.2}O_3$ (BSCF) was coated with CoO particles in different percentages 5-10% and calcined at 600°C. The cell performance was evaluated in an anode supported cell configuration 10%CoO with BSCF exhibited the highest power density of 463mW/cm^2 as compared to blank BSCF which 223mW/cm^2 at 550°C. The reason for this was the increased surface area of CoO coated BSCF, which facilitated the oxygen reduction reaction (ORR) [8]. The fuel cell electrochemical performance improved by providing a high surface area for reaction. A nanostructured BSCF cathode prepared by laser deposition. In this process, a BSCF target is ablated with a pulsed laser beam, and the

thin film of BSCF is deposited on the YSZ electrolyte at different temperatures. The crystallinity of the deposited films increased as the deposition temperature was 500-800°C. The Nano-structured films exhibited peak power of 55 mW/cm^2 at 450°C due to increased oxygen reduction sites [9]. A factor that affects the fuel cell electrode performance is its adhesion to the electrolyte, confirming a good electrode-electrolyte interface. A $Ba_{0.5}Sr_{0.5}Co_{0.8}Fe_{0.2}O_3$ - $Gd_{0.1}Ce_{0.9}O_{1.95}$ (BSCF-GDC) composite cathode was developed to counter the adhesion problem faced by a predecessor in which BSC-GDC cathode was electrospun. In this study, BSCF fibers were electro-spun and mixed with GDC powered for pasting on the GDC electrolyte. The mixed fibrous BSCF and GDC powder improved the adhesion, which attributed to a low shrinkage rate of 17.6% as compared to electrospun BSCF-GDC 18.1% during sintering and high surface area of 11.50 m^2/g. The electrochemical performance of the cathode was as follows 0.1 Ωcm^2 as compared to electro-spun BSCF-GDC 0.13 Ωcm^2 at 700°C. And power density of 500 mW/cm at 700°C , 25% more than conventional composite cathode [10]. The electrochemical performance of fuel cells can also improve through their microstructure e.g. finer particles, high porosity, and larger surface area. A $Ba_{0.5}Sr_{0.5}Co_{0.8}Fe_{0.2}O_3$ (BSCF) – $BaZr_{0.1}Ce_{0.7}Y_{0.2}O_3$ (BCYZ) was prepared and microwave sintered at 900°C for just 10 min as compared to conventional sintering which takes hours and a much larger temperature, this case its 1100°C for 2 hours. The microwave sintering resulted in a uniform microstructure ascribed to a uniform heating pattern. Also lowered sintering temperature alleviated Ba diffusion from electrolyte increasing ohmic resistance and reducing BSCF catalytic property due to Ba enrichment. The electrochemical results at 700°C indicated lower Ohmic and polarization resistances of 0.185 Ωcm^2 and 0.075 Ωcm^2 for microwave sintered BSCF at 900°C for 10 min, 0.29 Ωcm^{2,} and 0.11 Ωcm^2 for conventionally sintered at 1100°C for 2 hours. While the peak power densities were 0.96 W/cm^2 and 0.33 W/cm^2 for microwave and conventionally sintered cathodes [11]. Another study showed the surface area improvement influenced the electrochemical performance of the fuel cell. In this study, a mix of $Ba_{0.5}Sr_{0.5}Co_{0.8}Fe_{0.2}O_3$ (BSCF) nanotubes and nanoparticles were prepared with 10% and 20% nanotubes (NTs) mixed with nanoparticles (NPs). The incorporation of nanotube increased the porosity and 27% for 10% NTs and 35% for 20% NTs, and the surface area for 10% NTs was reported to be 15.02 m^2/g larger than NPs which is 9.28 m^2/g. The electrochemical results showed ASR for NTs-10%, NTs-20% and NPs were 0.06, 0.23, and 0.11 Ωcm^2 respectively at 800°C. This was

attributed to the larger surface area for NPs/NTs combination [12]. Another factor that affects cell performance is sintering temperature, which affects the morphology and crystal structure of the electrode. A $Ba_{0.5}Sr_{0.5}Co_{0.8}Fe_{0.2}O_3$ (BSCF) $-$ $Ce_{0.85}Sm_{0.15}O_3$ (SDC) composite cathode incorporated with CuO was prepared to improve its ionic conductivity. The SDC with 0.5% CuO was prepared and mixed with BSCF and sintered from 900°C, 950°C, and 1000°C. Prepares cathode material was screen printed on SDC electrolyte and an anode-supported cell was prepared. The comparison of BSCF, BSCF-SDC, and BCSF-SDC-CuO showed the addition of CuO enhanced the electrochemical properties of the composite. The power density and polarization at 800°C resistance value were 0.124 Ωcm^2 and 105.2 mW/cm^2, 0.051 Ωcm^2 and 210.6 mW/cm^2, and 0.048 Ωcm^2 and 352.5 mW/cm^2 respectively when sintered at 950°C [13].

2.3 Lanthanum Strontium Cobalt Ferrite

LSCF is perovskite material, which is a mixed ionic and electronic conductor with ionic, electronic conductivity, and catalytic activity for oxygen reduction. LSCF is an ideal material for the cathode in solid oxide fuel cell application. The cell performance as discussed earlier adjusted by controlling the morphology and microstructure of the cathode. A study was conducted to fabricate $La_{0.6}Sr_{0.4}Co_{0.2}Fe_{0.8}O_3$ (LSCF) was fabricate by using an inkjet printer in an anode-supported cell printed on YSZ electrolyte. A water-solvent-based ink was prepared with different amounts of solvent and luminosity adjusted from dark to bright to control the cathode structure e.g. the dark printed cathode showed large crackers due to slow solvent evaporation and brightly printed exhibited tight structure with small pores. The ink was prepared 0%, 10%, and 20% 1,5-pentanediol solvent and electrochemical results showed that sample with 20% solvent and brightly printed exhibited a power density of 377mW/cm² at 600°C [14].

In another study, a water-based electro-spun LSCF cathode was prepared and applied onto the GDC electrolyte surface. Three types of fibers spun with 55%, 59%, and 62% water content. Nanofibers with 62% water content were used because they retained the porosity value of 37.5% after heat treatment. The water-based electrospun nanofiber showed a low polarization resistance of 1 Ωcm^2 at 650°C attributed to extended triple-

phase boundary due to the high porosity of nanofiber cathodes [15]. Doping is a suitable element in cathode material can also improve the performance of cathode. In this study, cerium was doped in LSCF cathode to improve its performance. For this purpose the cathode material $La_{0.6-x}Ce_xSr_{0.4}Co_{0.2}Fe_{0.8}O_3$ synthesized by sol-gel method with x= 0-0.6. The structural analysis showed the Ce occupied A-site as its ionic radius is more similar to La. The polarization resistance values of the samples were 0.09, 0.14, and 0.21 Ωcm^2 for LSCF, LSCF3, and LSCF6 respectively at 750°C. This indicates as the Ce content increased in LSCF the oxygen vacancies enhanced and which in turn increased the reaction sites [16]. To improve the electro-catalytic activity of LSCF for solid oxide fuel cells. The surface of LSCF is decorated with CuO nanoparticles to improve its ORR activity. For this purpose, copper solution infiltrated dropwise on the porous LSCF surface and sintered at 800°C. The CuO particles addition enhanced the ORR by a factor of 4 at 750°C. The interfacial resistance reduced from 2.27 to 1.5 Ωcm^2 and peak power increased from 540 mW/m^2 to 720 mW/m^2 at 650°C [17].

2.4 Mixed Ions and Electrons Conducting Composite

In mixed ions and electrons conducting (MIEC) composite material, electron-conducting cathode and ion-conducting electrolyte materials are composited. In this way, the ionic and electronic conductivity of the cathode increased because of the enlargement of the electrochemical reactions zone. The structural stability, as well as adherence to the electrolyte, is improved. In a research study, LSM an MIEC, and Scandia stabilized zirconia (ScSZ) were used to prepare cathode material by mechanically mixing both in two ratios 22% and 50% ScSZ. In addition, electrolyte-supported cell configuration was used with ScSZ to evaluate the cell performance. The commercially available LSM-ScSZ and mechanically prepared materials were compared and the results exhibited that the commercially prepared sample with 50:50 weight percent of LSM and ScSZ showed a peak power of 0.32 W/cm^2 and interfacial polarization resistance of 0.50 Ωcm^2 at 800°C [18]. A $BaCe_{0.5}Zr_{0.35}Y_{0.15}O_3$-$La_{0.6}Sr_{0.4}Co_{0.2}Fe_{0.8}O_3$ (LSCF-BCZY) composite prepared by electrospinning a mixture of BCZY powder and LSCF sol-gel. The characterization study showed even dispersion of BCZY and incorporation with LSCF. The electrochemical studies showed those LSCF-BZCY composite peak power densities of 0.239 W/cm^2 at 550°C

and 0.537 W/cm^2 at 700°C. This attributed to the enhanced surface of electrospun composite 10.39 m^2/g as compared to conventional composite powder 4.58 m^2/g [19]. A comparative study conducted on La$_{0.6}$Sr$_{0.4}$Co$_{0.2}$Fe$_{0.8}$O$_3$ – Ce$_{0.8}$Sm$_{0.2}$O$_{1.9}$ (LSCF-SDC) composite with nano-sized and micro-sized particles. The prepared LSCF-SDC powered sintered at different temperatures 800-1200°C resulted in a range of particles from 1.2 microns to 50 nm. A symmetric cell configuration was used to evaluate the electrochemical properties of composite cathode prepared by LSCF solution infiltration into SDC porous scaffold LSCF-SDC/SDC/SDC-LSCF. The characterization results indicate that sintering temperature influenced the electrochemical performance of the symmetric cell. For instance, the ASR value of composite sintered at 1400°C for 4 hours was 2.1 Ωcm^2 with an average particle size of 1.2 microns and 0.21 Ωcm^2 for 800°C for 4 hours sintered composite with an average grain size of 50nm [20]. GDC provides be a good barrier between the LSCF and YSZ electrolyte to avoid a reaction. In research, LSCF and GDC nanocomposite cathodes were studied prepared by spray pyrolysis. LSCF and GDC composite were prepared with different LSCF content (LSCF= 100% - 50%) and co-sintered at 800-1000°C. For comparison with nanocomposite traditional screen-printed cathodes were also prepared. The electrochemical performance of single-cell and symmetric cells was examined. The polarization resistance was from 0.30 Ωcm^2 to 0.150 Ωcm^2 for 50%LSCF and 100%LSCF at 600°C ascribed to the fact the addition of GDC suppressed the grain growth and the average size was 30nm in case of 50%LSCF and 50nm 100%LSCF. In single-cell case, LSCF-GDC with 50%LSCF showed a power density of 900 mW/cm^2 to 560 mW/cm^2 for traditional screen-printed cathode [21]. A study was conducted to analyze the optimal amount of GDC in LSCF-GDC nanocomposite. LSCF was composited with varying amounts of GDC =30-70% and composite pellets were fabricated and sintered at 1100°C for 2 hours, for DC conductivity measurements. The crystallite size of GDC increased with increasing its content and hindered the LSCF size growth. The catalytic activity of nanocomposite is dependent on the surface area so, a nanocomposite with high GDC content is not recommended because it increased the amount of ion-conducting species but reduced the catalytic activity for the oxygen reduction reaction. The DC conductivity measurement showed 30 S/cm value and least activation energy .04 eV for 50% GDC [22]. LSCF-GDC composite cathodes were prepared using screen printing, electrospinning, and solution-infiltration method. The current density was used for the

stability test of the prepared cathode at 700ºC with a current density of 100mA/cm^2. After a test run of 144 hours, the electrospun LSCF-GDC nanocomposite cathode showed the minimum polarization resistance of 0.098 Ω/cm^2 [23]. In this study, LSCF nanoparticles and nanorods are used to prepare core-shell structured composite cathode. LSCF nanorods and nanoparticles were sprayed uniformly in a crucible and on top of LSCF, GDC was coated. The process was repeated several times and the resultant composite was heat-treated to get LSCF-GDC composite cathode. The cathode was screen-printed on one side GDC electrolyte, with Pt paste on the other side as the counter electrode. A stability test under 100 mA/cm^2 for 144 hours was performed showed constant polarization resistance. Even after 1242 hours it remained stable and polarization resistance decreased from 0.147 Ω/cm^2 to   0.129 Ω/cm^2[24]. LSCF cathode can react with the electrolyte material which can affect the electrode/electrolyte interface which is important for fuel cell performance. In this study, LSCF phase segregation on GDC and YSZ electrolytes was studied. LSCF was assembled onto electrolyte with Pt paste as counter and reference electrodes. Zr in YSZ acts as a catcher and driving force for reaction with Sr forming SrZrO$_3$ which disintegrates the LSCF structure. In the case of GDC, no catcher exists so the Sr segregation process becomes slow as compared to YSZ. In conclusion, chemical catchers of segregated species act as driving forces for and affect the LSCF electrode structure [25].

2.5 Objectives of this Study

In the context of a detailed review of literature, the objectives of this study are given below:

- Synthesis of lanthanum strontium cobalt ferrite (LSCF, $La_{0.6}Sr_{0.4}Co_{0.2}Fe_{0.8}O_3$) and Gadolinium doped-ceria (GDC, $Gd_{0.1}Ce_{0.9}O_{1.95}$) employing solution combustion synthesis
- LSCF-GDC nanocomposite synthesis
- LSCF-GDC nanocomposite cathode pellet synthesis by uniaxial hydraulic pressing
- Structural evaluation of the prepared LSCF-GDC nanocomposite and comparison with literature
- Reporting the electrical transport of LSCF-GDC nanocomposite prepared by conventionally and microwave sintering method

Summary

LSCF perovskite-based cathode materials are good candidates for intermediate temperature solid oxide fuel cell applications (IT-SOFC). The LSCF possesses both ionic and electronic conductivity but pure LSCF's ionic conductivity is low to use as an efficient cathode material for IT-SOFC, a composite of LSCF-GDC is used. GDC is chemical stable with LSCF and a good thermal expansion coefficient match. For this purpose, a 10% gadolinium doped ceria is used. The use of GDC with LSCF has proven its chemical compatibility and enhanced electrochemical performance. The study, objectives are to develop a nanocomposite material for intermediate temperature solid oxide fuel cell applications.

References

[1]   T. Noh, J. Ryu, J. Kim, Y. N. Kim, and H. Lee, "Structural and impedance analysis of copper doped LSM cathode for IT-SOFCs," *J. Alloys Compd.*, vol. 557, pp. 196–201, 2013, DOI: 10.1016/j.jallcom.2013.01.002.

[2]   S. W. Baek *et al.*, "Metal-supported SOFC with an aerosol deposited in-situ LSM and 8YSZ composite cathode," *Ceram. Int.*, vol. 42, no. 2, pp. 2402–2409, 2016, DOI: 10.1016/j.ceramint.2015.10.039.

[3]   O. O. Agbede, K. Hellgardt, and G. H. Kelsall, "Electrical conductivities and microstructures of LSM, LSM-YSZ and LSM-YSZ/LSM cathodes fabricated on YSZ electrolyte hollow fibers by dip-coating," *Mater. Today Chem.*, vol. 16, p. 100252, 2020, DOI: 10.1016/j.mtchem.2020.100252.

[4]   J. W. Park and K. T. Lee, "Enhancing performance of $La_{0.8}Sr_{0.2}MnO_3$ infiltrated $Er_{0.4}Bi_{1.6}O_3$ cathodes via controlling wettability and catalyst loading of the precursor solution for IT-SOFCs," *J. Ind. Eng. Chem.*, vol. 60, pp. 505–512, 2018, DOI: 10.1016/j.jiec.2017.11.039.

[5]   M. V. Sandoval, C. Cárdenas, E. Capone, C. Pirovano, P. Roussel, and G. H. Gauthier, "Performance of $La_{0.5}Sr_{1.5}MnO_{4\pm\delta}$ Ruddlesden-Popper manganite as electrode material for symmetrical solid oxide fuel cells. Part A. The oxygen reduction reaction," *Electrochim. Acta*, vol. 304, pp. 415–427, 2019, DOI: 10.1016/j.electacta.2019.03.037.

[6]   S. He *et al.*, "Interface formation and Mn segregation of directly assembled $La_{0.8}Sr_{0.2}MnO_3$ cathode on Y_2O_3-ZrO_2 and Gd_2O_3-CeO_2 electrolytes of solid oxide fuel cells," *Solid State Ionics*, vol. 325, no. August, pp. 176–188, 2018, DOI: 10.1016/j.ssi.2018.08.016.

[7]   C. H. Chen, C. L. Chang, and B. H. Hwang, "Electrochemical and microstructure characteristics of $Ba_{0.5}Sr_{0.5}Co_{0.8}Fe_{0.2}O_{3-\delta}$ (BSCF) cathodes prepared by citrate precursor method for SOFCs," *Mater. Chem. Phys.*, vol. 115, no. 1, pp. 478–482, 2009, DOI: 10.1016/j.matchemphys.2009.01.018.

[8]   Y. He *et al.*, "Cobalt oxides coated commercial $Ba_{0.5}Sr_{0.5}Co_{0.8}Fe_{0.2}O_{3-\delta}$ as high performance cathode for low-temperature SOFCs," *Electrochim. Acta*, vol. 191, pp. 223–229, 2016, doi: 10.1016/j.electacta.2016.01.090.

[9]   Y. Li, L. M. Wong, C. C. Yu, S. Wang, and P. C. Su, "Pulsed laser deposition of $Ba_{0.5}Sr_{0.5}Co_{0.8}Fe_{0.2}O_{3-\delta}$ thin film cathodes for low-temperature solid oxide fuel cells," *Surf. Coatings Technol.*, vol. 320, pp. 344–348, 2017, doi: 10.1016/j.surfcoat.2016.12.051.

[10]   S. Lee, K. Lee, S. Kang, J. Kang, S. Song, and J. Bae, "Investigation of electrospun $Ba_{0.5}Sr_{0.5}Co_{0.8}Fe_{0.2}O_{3-\Delta}$-$Gd_{0.1}Ce_{0.9}O_{1.95}$ cathodes for enhanced interfacial adhesion," *Int. J. Hydrogen Energy*, vol. 43, no. 46, pp. 21535–21546, 2018, doi: 10.1016/j.ijhydene.2018.09.130.

[11]   W. Liu, H. Kou, X. Wang, L. Bi, and X. S. Zhao, "Improving the performance of the $Ba_{0.5}Sr_{0.5}Co_{0.8}Fe_{0.2}O_{3-\delta}$ cathode for proton-conducting SOFCs by microwave sintering," *Ceram. Int.*, vol. 45, no. 16, pp. 20994–20998, 2019, doi: 10.1016/j.ceramint.2019.06.281.

[12]   A. S. Habiballah, N. Osman, and A. M. Md Jani, "Microstructural investigation of BSCF-based cathode material for enhanced oxygen reduction reaction performance and electrode stability," *Ceram. Int.*, vol. 46, no. 14, pp. 23262–23265, 2020, doi: 10.1016/j.ceramint.2020.06.002.

[13]   S. Zhao, N. Tian, and J. Yu, "cathode for intermediate temperature solid oxide fuel cells," vol. 825, pp. 0–4, 2020.

[14]   G. D. Han *et al.*, "Fabrication of lanthanum strontium cobalt ferrite (LSCF) cathodes for high performance solid oxide fuel cells using a low price commercial inkjet printer," *J. Power Sources*, vol. 306, pp. 503–509, 2016, doi: 10.1016/j.jpowsour.2015.12.067.

[15]   A. Enrico, W. Zhang, M. Lund, E. Marzia, P. Costamagna, and P. Holtappels, "Journal of the European Ceramic Society solid oxide fuel cells by water-based sol-gel electrospinning : Synthesis and electrochemical behaviour," vol. 38, no. January, pp. 2677–2686, 2018.

[16]   F. Zhou *et al.*, "Effects of cerium doping on the performance of LSCF cathodes for intermediate temperature solid oxide fuel cells," *Int. J. Hydrogen Energy*, vol. 43, no. 41, pp. 18946–18954, 2018, doi: 10.1016/j.ijhydene.2018.08.041.

[17]   T. Hong, K. Brinkman, and C. Xia, "Copper oxide as a synergistic catalyst for the oxygen reduction reaction on $La_{0.6}Sr_{0.4}Co_{0.2}Fe_{0.8}O_{3-\delta}$ perovskite structured electrocatalyst," *J. Power Sources*, vol. 329, pp. 281–289, 2016, doi: 10.1016/j.jpowsour.2016.08.075.

[18]   K. Hosokawa, A. Kondo, M. Okumiya, H. Abe, and M. Naito, "One-step mechanical processing to prepare LSM/ScSZ composite particles for SOFC cathode," *Adv. Powder Technol.*, vol. 25, no. 5, pp. 1430–1434, 2014, doi: 10.1016/j.apt.2013.12.006.

[19]   S. Lee, S. Park, S. Wee, H. woo Baek, and D. Shin, "One-dimensional structured $La_{0.6}Sr_{0.4}Co_{0.2}Fe_{0.8}O_{3-\delta}$ - $BaCe_{0.5}Zr_{0.35}Y_{0.15}O_{3-\delta}$ composite cathode for protonic ceramic fuel cells," *Solid State Ionics*, vol. 320, no. March, pp. 347–352, 2018, doi: 10.1016/j.ssi.2018.03.010.

[20]   H. Xu, H. Zhang, and A. Chu, "An investigation of oxygen reduction mechanism in nano-sized LSCF-SDC composite cathodes," *Int. J. Hydrogen Energy*, vol. 41, no. 47, pp. 22415–22421, 2016, doi: 10.1016/j.ijhydene.2016.09.153.

[21]   D. Szymczewska, J. Karczewski, A. Chrzan, and P. Jasinski, "CGO as a barrier layer between LSCF electrodes and YSZ electrolyte fabricated by spray pyrolysis for solid oxide fuel cells," *Solid State Ionics*, vol. 302, pp. 113–117, 2017, doi: 10.1016/j.ssi.2016.11.008.

[22]   A. P. Jamale, S. T. Jadhav, S. U. Dubal, C. H. Bhosale, and L. D. Jadhav, "Studies on the percolation limit of $Ce_{0.9}Gd_{0.1}O_{1.95}$ in $La_{0.6}Sr_{0.4}Co_{0.2}Fe_{0.8}O_{3-\delta}$-$Ce_{0.9}Gd_{0.1}O_{1.95}$ nanocomposites for solid oxide fuel cells application," *J. Phys. Chem. Solids*, vol. 85, pp. 96–101, 2015, doi: 10.1016/j.jpcs.2015.05.012.

[23]   D. Li, Y. Jin, C. Liu, M. Fu, X. Zong, and Y. Xiong, "Effect of optimal GDC loading on long-term stability of $La_{0.8}Sr_{0.2}Co_{0.2}Fe_{0.8}O_{3-\delta}/Gd_{0.2}Ce_{0.8}O_{1.9}$ composite cathodes," Ceram. Int., vol. 47, no. 5, pp. 6591–6596, 2021, doi:

10.1016/j.ceramint.2020.10.248.

[24] D. Li et al., "Study on durability of novel core-shell-structured $La_{0.8}Sr_{0.2}Co_{0.2}Fe_{0.8}O_{3-\delta}@Gd_{0.2}Ce_{0.8}O_{1.9}$ composite materials for solid oxide fuel cell cathodes," Int. J. Hydrogen Energy, vol. 46, no. 55, pp. 28221–28231, 2021, doi: 10.1016/j.ijhydene.2021.06.031.

[25] Y. Sun, S. He, M. Saunders, K. Chen, Z. Shao, and S. P. Jiang, "A comparative study of surface segregation and interface of $La_{0.6}Sr_{0.4}Co_{0.2}Fe_{0.8}O_{3-\delta}$ electrode on GDC and YSZ electrolytes of solid oxide fuel cells," Int. J. Hydrogen Energy, vol. 46, no. 2, pp. 2606–2616, 2021, doi: 10.1016/j.ijhydene.2020.10.113.

Chapter 3

Review on Experimentation and Characterization Methods

This chapter will cover the review techniques employed for the synthesis of material and characterization techniques used commonly for analysis of the synthesized materials.

3.1 Wet Chemistry Synthesis

The wet chemistry route involves homogeneous mixing at the atomic level. This method gives complete control over particulate size, powder morphology, and surface area. The advantages of this method are high surface area, low temperature as well as no impurity phase. The main examples of wet chemistry are sol-gel synthesis, solution combustion synthesis, hydrothermal synthesis, etc.

3.1.1 Sol-gel Synthesis Method

The sol-gel method involves a network called gel formed from a solution. This method enables homogeneity at the molecular level. The composition of product material can be tailored easily by different precursor ratios in the solution. This method is parameter sensitive such as temperature and pH of the solution as well as reactant composition and solvent nature. Sol is short for the solution, it is colloidal of particles for the synthesis of nanoparticles. The solution is formed when the precursor solution undergoes condensation and hydrolysis. Metal chlorides and alkoxides are commonly used in this technique. The first step in this method is hydrolysis in which, the metal center is connected with O or OH. In the next step, the liquid is removed from the solution forming a porous structure (gel) called the condensation step. Afterward, the gel is dried, it gives rise to the final powder product. The advantages of this method are low temperature and homogeneous product [1].

3.1.2 Solution Combustion Synthesis

Solution combustion synthesis is a popular method for the synthesis of nanomaterials. It is a self-propagating synthesis process. There are three classifications based on the initial reaction mediums as follow:

1. Solid-state reactants
2. Initial reactants as an aqueous solution
3. Gas-phase combustion

It is a simple, easy, and rapid process for nanocomposite in which self-sustained reaction occurs between nitrates and fuel e.g. urea, glycine, and citric acid. In solution, combustion synthesis solution is heated employing an external source, which heats the solution to ignition temperature and self-propagating reaction is started, and solid product is obtained[11].

3.1.3 Co-precipitation Synthesis

The co-precipitation method is simple and used to prepare less clustered and well-defined oxide products. It involves stirring of the precursor solutions followed by nucleation and growth, agglomeration of particles, precipitation, filtration, and calcination of the final product. In this method, nucleation is the main step in which small particles are formed. The precipitation begins at certain pH and resulted in a precipitate which filtered, washed several times, and dried in an oven. The product's properties such as particle size, morphology depend upon secondary activities e.g. Ostwald ripening & aggregation [2].

3.1.4 Hydrothermal Synthesis

Hydrothermal synthesis uses pressurized and hot water for the precipitation of anhydrous and crystallized ceramic powders. This technique replaces the calcination procedure required in sol-gel and coprecipitation methods with hydrothermal reaction. The procedure involves the dissolution of precursors separately and mixing with precipitant. The precipitated gel was sealed in an autoclave reactor and heated in an oven. Then acquired powder is washed and dried in the air. This is a simple method and many phases can be prepared at low temperatures [3].

3.2 Solid State Synthesis

The solid-state method is commonly used for the synthesis of material due to its simplicity and energy efficiency. In this method is solid powdered materials are mechanically mixed and annealed afterward. The solid-state method involves direct interaction between precursors materials and no decomposition is involved [3]. The method involves

- Proper selection of material that is not inert and in of fine powders or particles
- Stoichiometric proportionate amounts of precursor materials
- Through mixing of materials by hand or a ball mill
- After that heat treatment of obtained material at the required temperature

Besides the simplicity and ease of the method, there are some drawbacks involved [2]

- High calcination temperature
- Poor homogeneity
- Non-uniform size distribution
- Low surface area

3.4 Characterization Techniques

In material science, characterization techniques are used to identify materials, analyze material morphology, and microstructure. In this section brief introduction of commonly used characterization, techniques will be discussed.

3.4.1 X-Ray Diffraction

X-ray diffractometers use x-ray which is produced when a high energy beam of electrons accelerates through a high voltage field and incidents on a solid target of molybdenum or copper. These X-rays are used to extract the structural information of the material. When radiation from a source strikes the material, it will be either scattered or absorbed. When it strikes elastically with the material e.g. no energy is lost and the wavelength of the incident radiation remains unchanged. The arrays of the atoms in the lattice of the target material will interact with radiation and will be

scattered as shown in figure 3.1. A function plotted between the intensity of the radiation and the angle of scattering resulting in a spectrum [6].
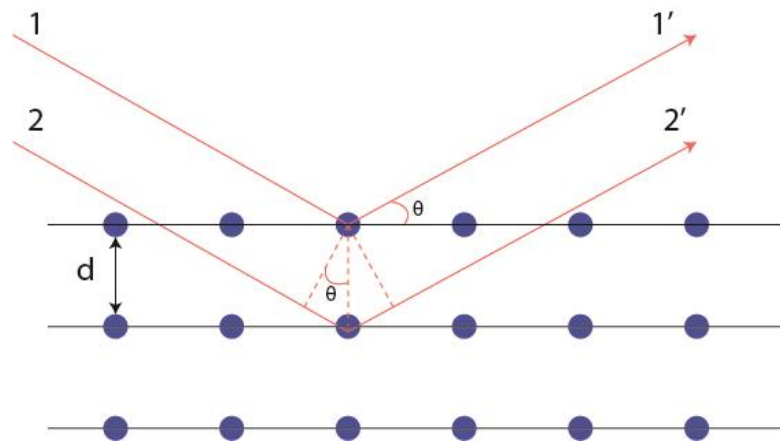

Figure 3.1: A visual representation of X-ray diffraction in lattice planes [6]

This spectrum is matched with the diffraction standard JCPDS files to identify the material. Bragg's law governs the interaction of radiation and scattering its scattering from an array, which is as follow:

$$n\lambda = 2d\sin\theta \ \ldots\ldots\ldots\ldots\ldots.(3.1)$$

Where "λ" is the wavelength of radiation, "θ" is the diffraction angle which incident beam makes with lattice points, "n" is an integer called an order of reflection [9]

We can calculate the crystallite size of the material using the Debye Scherrer equation:

$$D = \frac{0.9\lambda}{\beta\cos\theta} \ \ldots\ldots\ldots\ldots\ldots. \ (3.2)$$

Where "D" is crystallite size, "λ" is the wavelength of radiation, "θ" is diffraction angle, and "β" is full width half maximum (FWHM)[13].

3.4.2 Scanning Electron Microscopy (SEM)

SEM is a powerful technique for material characterization such as microstructure, crystalline structure, and shape, orientations, defects in crystals, atoms distribution, morphology, and chemistry. It can achieve higher resolution than optical microscopes because the wavelength of electrons is 100,000 times shorter than visible light. The

scattering of incident electrons beam after targeting the materials can be elastic for image measurements or inelastic for spectroscopy. In the case of inelastic interaction, incident electron beams interact with electrons and during an elastic collision, they interact with the nucleus. When these electrons interact elastically or in-elastically, they lose transfer the of energy to electrons. If the energy is less than 50eV these will be called secondary electrons (SE) and SE mostly emitted near the surface of material within a few nanometers depth. If the energy of emitted electrons is more than 50eV then these are called backscattered electrons (BSE) the signals generated by the interaction with samples are shown in figure 3.2. The images produced in SEM analysis are of three types [7]:

- Secondary electron
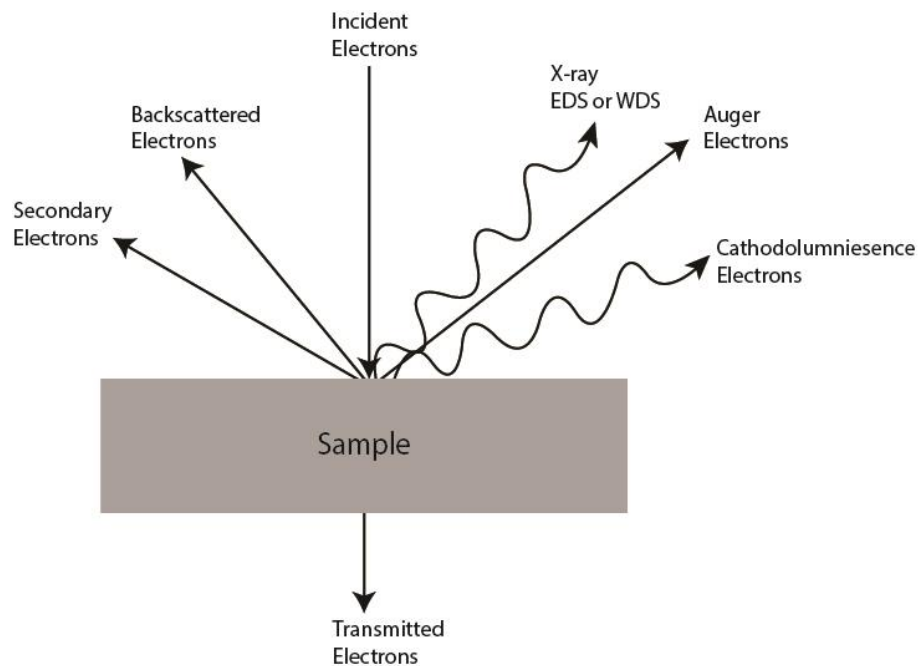- Backscattered electron
- Elemental X-ray map

Figure 3.2: Signals generated when incident electrons beam interact with sample [8]

The image formation is accomplished by mapping the BSE or SE signals intensity on the screen. The scan generator continually focuses the beam of the electrons on the specimen thus the intensity is mapped point to point on the cathode ray tube (CRT) or recorder. This intensity is translated into grayscale, the greater the intensity brighter will be the image. Magnification of SEM depends upon the area under scanning. As

the points displayed on the monitor are the array of the pixels, so smaller the area greater will be the magnification. An SEM ranges from 10x to 100kx. A typical SEM schematic is shown in figure 3.2 [9].
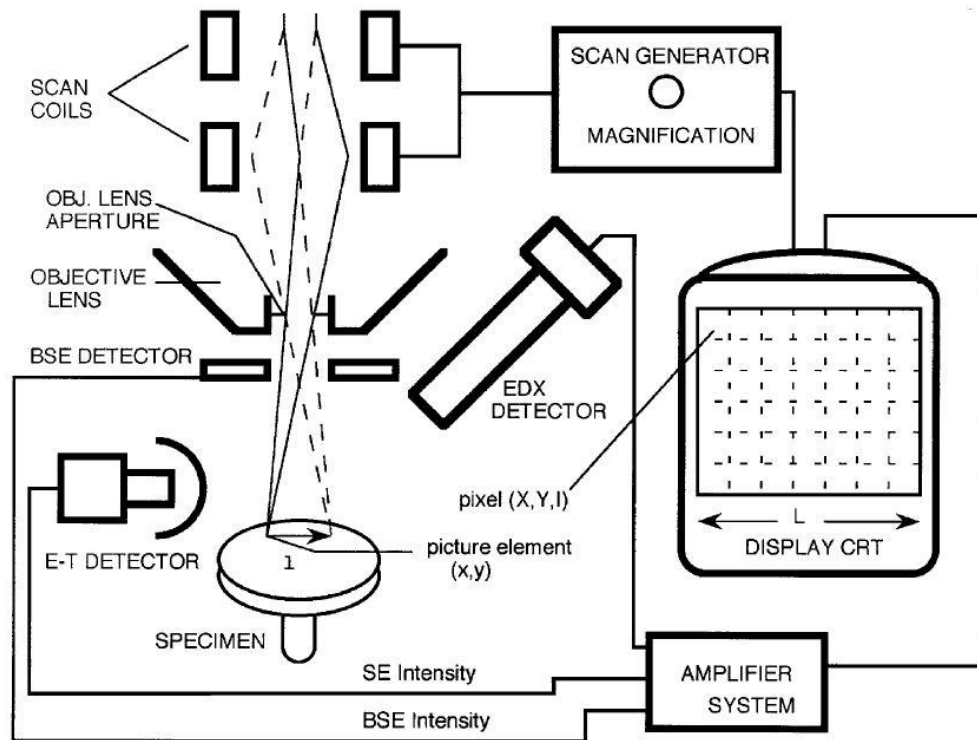

Figure 3.3: A schematic of scanning electron microscopy (SEM) [9]

3.4.3 Energy Dispersive Spectroscopy (EDS)

Electron microscopy utilizes high-energy electrons to analyze the specimen. When these electrons interact with the material they lose energy and are accompanied by X-rays, these losses represent the electrons' energy level in a specimen. Energy loss spectra are used to determine the composition of the specimen under observation. The X-rays can be used to analyze the elemental distribution in a specimen using energy dispersive spectroscopy (EDS). When electrons interact with sample photons are emitted lithium drifted silicon detector records the pulse which is proportional to the energy of an incident photon. As the incident photon reaches the detector ionization starts, the charge is developed which is directly proportional to photon energy, detected a pulse of current, and digitized to form energy spectra. EDS can be used to detect the elements from atomic numbers 4 to 92 namely beryllium and uranium[8].

3.4.4 AC Measurements

AC measurements were performed on two probe LCR meter. The ac conductivity was calculated by recording the impedance at 300-600°C. The prepared pellet was placed in the sample holder with two copper plates. Then sample holder was placed in the furnace and heated to 600°C. The reading was recorded with 50°C increments. The Figure 3.4 shows the AC measurements setup at high temperature.
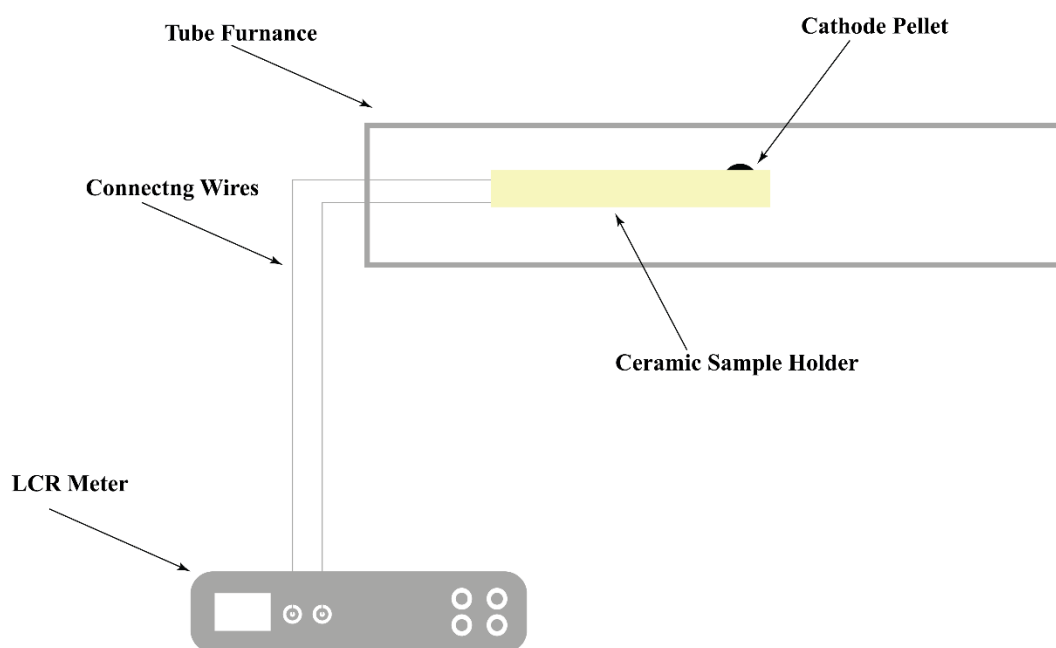

Figure 3.4: AC Measurement Scheme

Summary

In this chapter, a brief account of the synthesis methods for material and characterization techniques is given. For materials synthesis wet chemistry route, solid-state route or film deposition techniques can be employed, these methods come with pros and cons. For instance, the wet chemistry route offer controllability on materials properties such as morphology, particle size, and homogeneity. Whereas the solid-state route is facile but with some cons such as high sintering temperatures, non-homogeneity, and wide size distribution. Thin-film deposition techniques are also used for deposition of the thin layer directly on a substrate such as physical vapor deposition (PVD), chemical vapor deposition, and sputtering For the characterization of materials, X-ray diffraction is used for phase identification. The electron microscopy techniques use the emitted electrons from sample material to analyze materials. In this regard, SEM is used for structural analysis, EDS is used for elemental mapping, and Electrical measurements were performed on two probe LCR meter.

References

[1]   C.J. Brinker; G. W. Scherer, "Sol-Gel Science The physics and chemistry of Sol-gel processing -Brinker 1990.pdf." p. 462, 1990, DOI: 10.1016/S0254-0584(02)00315-2.

[2]   Z. Shao, W. Zhou, and Z. Zhu, "Advanced synthesis of materials for intermediate-temperature solid oxide fuel cells," *Prog. Mater. Sci.*, vol. 57, no. 4, pp. 804–874, 2012, DOI: 10.1016/j.pmatsci.2011.08.002.

[3]   W. A. Dollase, Solid-state chemistry and its applications by A. R. West, vol. 41, no. 6. 1985.

[4]   J. George, Preparation of Thin Films. 1992.

[5]   M. Ohring, "Material Science of Thin Films," *Igarss 2014*, no. 1, pp. 1–5, 2014.

[6]   J. J. Shea, Microstructural characterization of materials [Book Reveiw], vol. 16, no. 2. 2005.

[7]   G. C. Smith, "Concise encyclopedia of materials characterization," *Int. Mater. Rev.*, vol. 39, no. 1, pp. 48–48, 1994, DOI: 10.1179/imr.1994.39.1.48.

[8]   D. Brandon and W. D. Kaplan, Microstructural Characterization of Materials: 2nd Edition. 2008.

[9]   Elton N. Kaufmann, Characterization of Materials, 2 Volume Set-Wiley-Interscience (2003).

[10]   P. Gnanavel, S. Poongodi, and T. Ananthakrishnan, "Characterization techniques," *Man-Made Text. India*, vol. 53, no. 2, pp. 52–57, 2010, DOI: 10.1201/9781003148531-5.

[11]   B. D. Stojanovic, A. S. Dzunuzovic, and N. I. Ilic, Review of methods for the preparation of magnetic metal oxides. Elsevier Inc., 2018.

[12] C. G. Kumar, S. Pombala, Y. Poornachandra, and S. V. Agarwal, Synthesis, characterization, and applications of nanobiomaterials for antimicrobial therapy. Elsevier Inc., 2016.

[13] C. G. Kumar, S. Pombala, Y. Poornachandra, and S. V. Agarwal, Synthesis, characterization, and applications of nanobiomaterials for antimicrobial therapy. Elsevier Inc., 2016

Chapter 4

Experimentation

This chapter accounts for the experiments held during research to achieve the aforementioned study objectives. The experimentation includes the following:

- Synthesis of Lanthanum strontium cobalt ferrite (LSCF)
- Synthesis of Gadolinium-doped ceria (GDC)
- Synthesis of LSCF-GDC nanocomposite
- Fabrication of LSCF-GDC cathode pellet
- Microwave and conventional sintering of LSCF-GDC cathode for electrical performance comparison study

4.1 LSCF Synthesis

The LSCF perovskite $La_xSr_{1-x}Co_yFe_{1-y}O_3$ was prepared by employing solution combustion synthesis with $x=0.6$ and $y=2$. Precursor material in form of nitrate $La(NO_3)_3.6H_2O$, $Sr(NO_3)_2$, $Co(NO_3)_3$, and $Fe(NO_3)_3.6H_2O$ in molar ratio 6:4:2:8 were dissolved into de-ionized water using a magnetic stirrer. After the complete dissolution of material glycine fuel was added in the molar ratio of 3:1 to nitrates [1]. When glycine was completely dissolved in the solution the solution was heated on the hot plate at 90^oC until the solution was converted into the gel. The gel was transferred on a pre-heated hotplate at 300^oC. After few moments a combustion reaction started and the gel was converted into brownish ash. This ash was collected and calcined at 800^oC for 5 hours in the air the prepared sample is shown in figure 4.2 After calcination, a black powder was obtained. The process flow diagram is shown in figure 4.1. The calcined powder was characterized by XRD to determine the phase purity and structure of the crystal. XRD pattern was obtained using Copper-Kα radiation with a wavelength of $\lambda = 1.5425$Å with 2Θ in range of 10° to 80°.

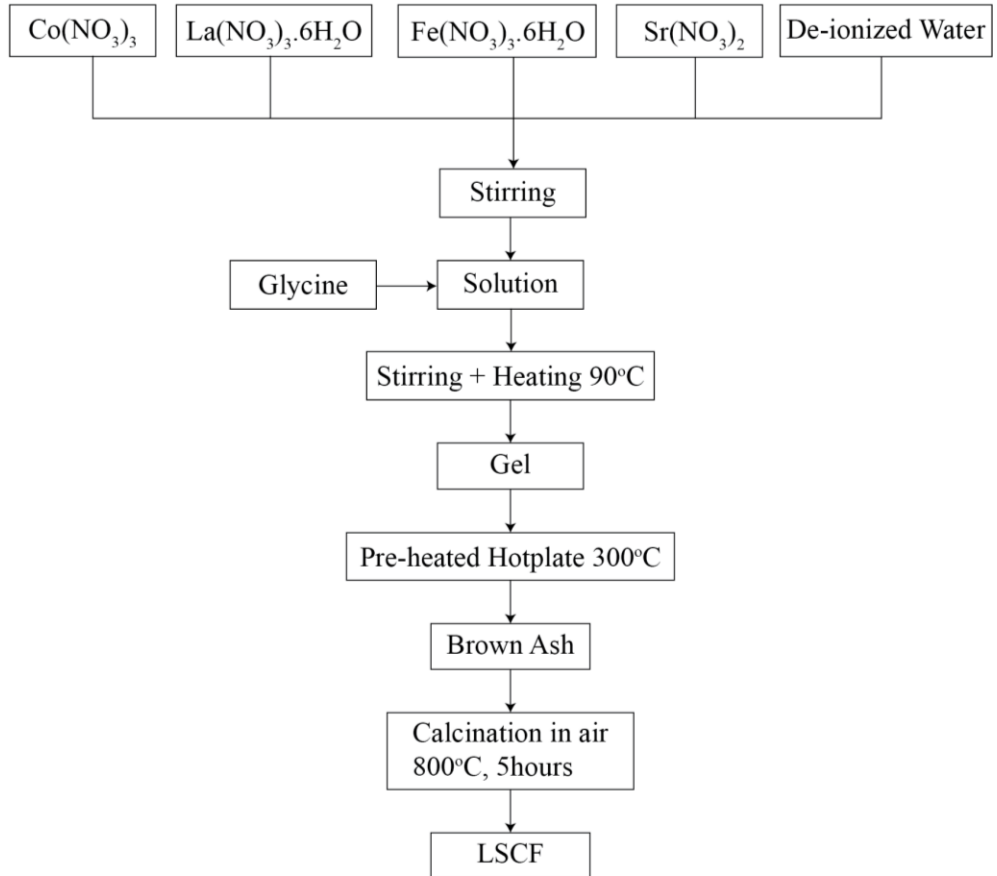**Figure 4.1:** Process flow diagram of LSCF synthesis via solution combustion method

Figure 4.2: Lanthanum strontium cobalt ferrite (LSCF) powder

4.2 GDC Synthesis

Gadolinium doped ceria $Ce_{0.9}Gd_{0.1}O_2$ was synthesis by using the solution combustion method. For this purpose $Ce(NO_3)_3 \cdot 6H_2O$ and $Gd(NO_3)_3 \cdot 6H_2O$ were completely dissolved in de-ionized water in a 9:1 molar ratio. Process flow for GDC synthesis is illustrated in figure 4.4. Later glycine was added in a ratio of 1.66:1 and dissolved in the solution [2]. This solution was placed on a hotplate at $90^{\circ}C$ with continuous stirring. Stirring was continued until white gel was formed, this gel was transferred to a pre-heated hotplate at $300^{\circ}C$. A combustion reaction started and the gel was converted into light-yellow ash. This ash was collected and placed into a muffle furnace in the air at $700^{\circ}C$ for 2 hours to get GDC powder. The prepared powder sample is shown in figure 4.3. Phase identification and structure were determined using XRD at an angle ranging between 10°-80° using copper-Kα radiations.

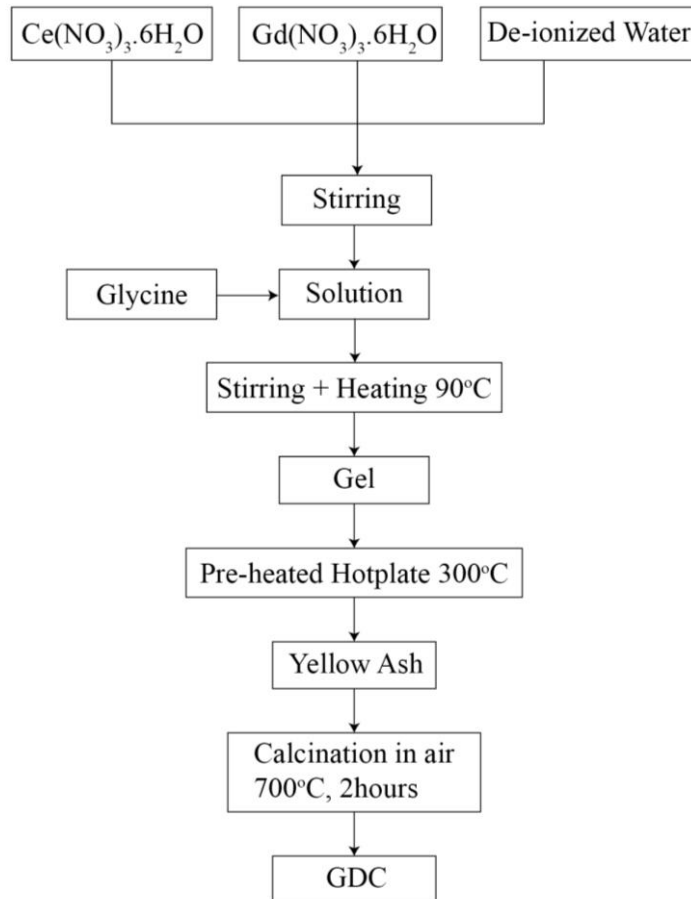**Figure 4.3:** Gadolinium doped-ceria (GDC) powder

Figure 4.4: Process flow diagram for GDC synthesis via solution combustion method

4.3 LSCF-GDC nanocomposite Synthesis

Figure 4.6 is given showing the process flow for LSCF-GDC nanocomposite preparation. LSCF-GDC nanocomposite was prepared by mixing LSCF and GDC powder in a weight ratio of 50:50 using mortar and pestle in the 2-propanol medium for 2 hours. Then the mixture was dried in the oven at 100°C for 30 min to evaporate the solvent before sintering [3]. Then the dried powder was sintered in a muffle furnace at 700°C for 2 hours at a heating rate of 5°C/min to obtain the final product. The synthesized nanocomposite powder is shown in figure 4.5. The XRD at 10-80° was performed for phase identification.

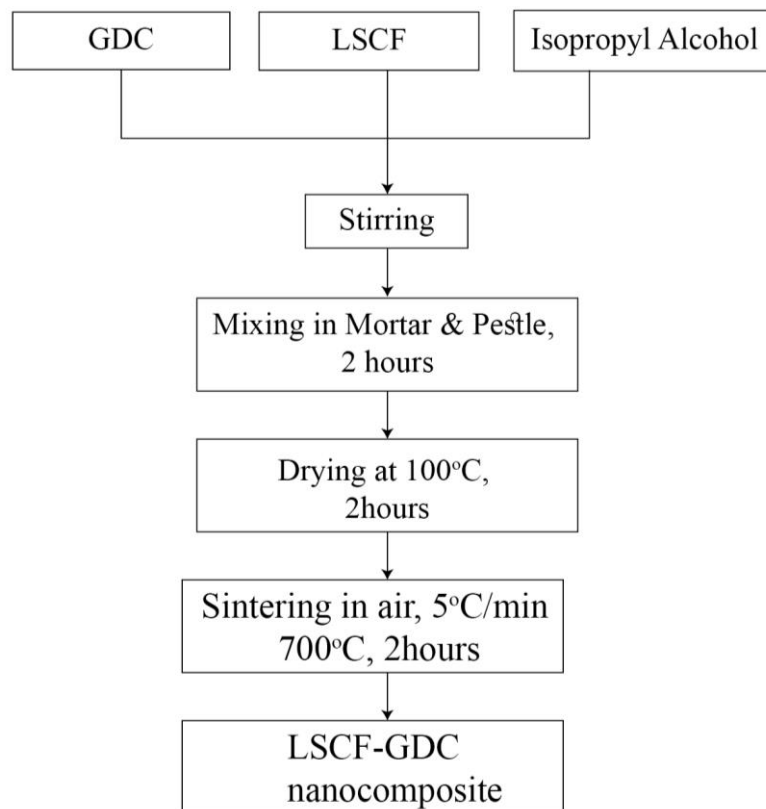**Figure 4.5:** Process flow diagram of LSCF-GDC nanocomposite synthesis

Figure 4.6: Process flow diagram of LSCF-GDC nanocomposite synthesis

4.4 LSCF-GDC Cathode Fabrication

The cathode pellet was fabricated LSCF-GDC powder. LSCF-GDC powder was ground before rolling into the pellet. Then the powder was uniaxially pressed under 15 MPa force for 90 seconds into 13mm circular disks. These green pellets were sintered in a resistive heating muffle furnace at 1100°C for 2 hours at 3°C/min and in a microwave furnace at 1100°C for 2 hours at 10°C/min. Figure 4.7 is given illustrating the process flow for GDC electrolyte pellet preparation. The as-prepared and sintered pellets are shown in figure 4.8. SEM technique was used for cross-sectional analysis and to assess the densification of the pellet.
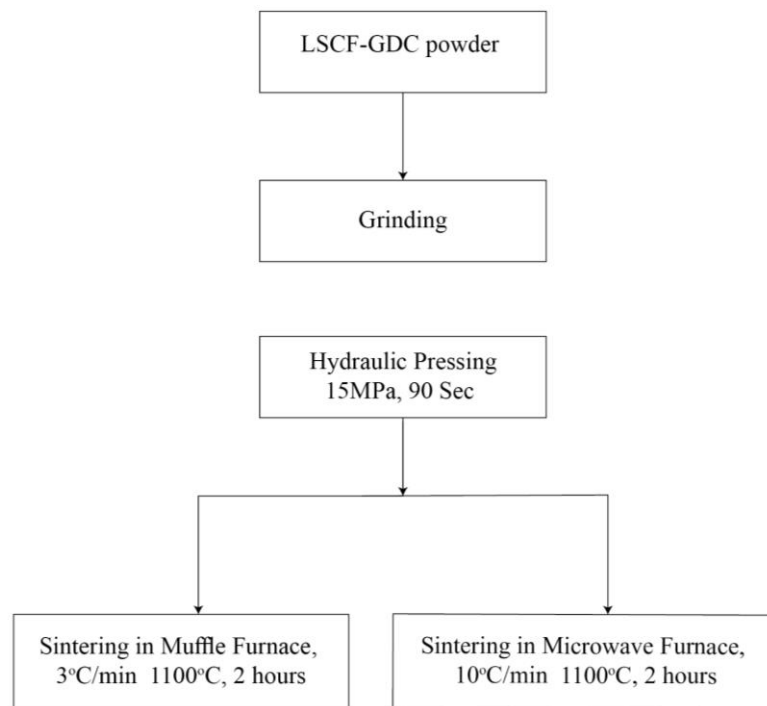

Figure 4.7: Process flow diagram for LSCF-GDC cathode pellet fabrication

Figure 4.8: As prepared pellet (left) and sintered (right)

Summary

This chapter accounts for the synthesis of LSCF and GDC nanocomposite material both powders were synthesized separately through solution combustion synthesis. LSCF-GDC composite was prepared by the solid-state route. The characterization of prepared material was performed using XRD and SEManalysis to determine phase, and cross-sectional analysis respectively. The cathode pellet of the LSCF-GDC pellet was fabricated and sintered employing microwave and the conventional furnace for comparison. The AC measurements were carried out between 300°-600°C.

References

[1]   S. A. Muhammed Ali, M. Anwar, M. R. Somalu, and A. Muchtar, "Enhancement of the interfacial polarization resistance of $La_{0.6}Sr_{0.4}Co_{0.2}Fe_{0.8}O_{3-\delta}$ cathode by microwave-assisted combustion method," Ceramics International, vol. 43, no. 5. pp. 4647–4654, 2017, doi: 10.1016/j.ceramint.2016.12.136.

[2]   S. A. Kumar, P. Kuppusami, and P. Vengatesh, "Auto-combustion synthesis and electrochemical studies of $La_{0.6}Sr_{0.4}Co_{0.2}Fe_{0.8}O_{3-\delta}$ – $Ce_{0.8}Sm_{0.1}Gd_{0.1}O_{1.90}$ nanocomposite cathode for intermediate temperature solid oxide fuel cells," Ceram. Int., vol. 44, no. 17, pp. 21188–21196, 2018, doi: 10.1016/j.ceramint.2018.08.164.

[3]   A. P. Jamale, S. T. Jadhav, S. U. Dubal, C. H. Bhosale, and L. D. Jadhav, "Studies on the percolation limit of $Ce_{0.9}Gd_{0.1}O_{1.95}$ in $La_{0.6}Sr_{0.4}Co_{0.2}Fe_{0.8}O_{3-\delta}$-$Ce_{0.9}Gd_{0.1}O_{1.95}$ nanocomposites for solid oxide fuel cells application," Journal of Physics and Chemistry of Solids, vol. 85. pp. 96–101, 2015, doi: 10.1016/j.jpcs.2015.05.012.

Chapter 5

Results and Discussion

This chapter includes detailed results and a discussion on the experiments to give the concluding remarks and recommendations at the end of the dissertation.

5.1 XRD Analysis

5.1.1 Lanthanum Strontium Cobalt Ferrite ($La_{0.6}Sr_{0.4}Co_{0.8}Fe_{0.2}O_3$)

Fig 5.1 shows the X-Ray diffractograms of the lanthanum strontium cobalt ferrite (LSCF) calcined at 800oC for 5 hours in the air. All the peaks are associated with rhombohedral perovskite structure and matched with PDF Card # 01-081-9113 [1].
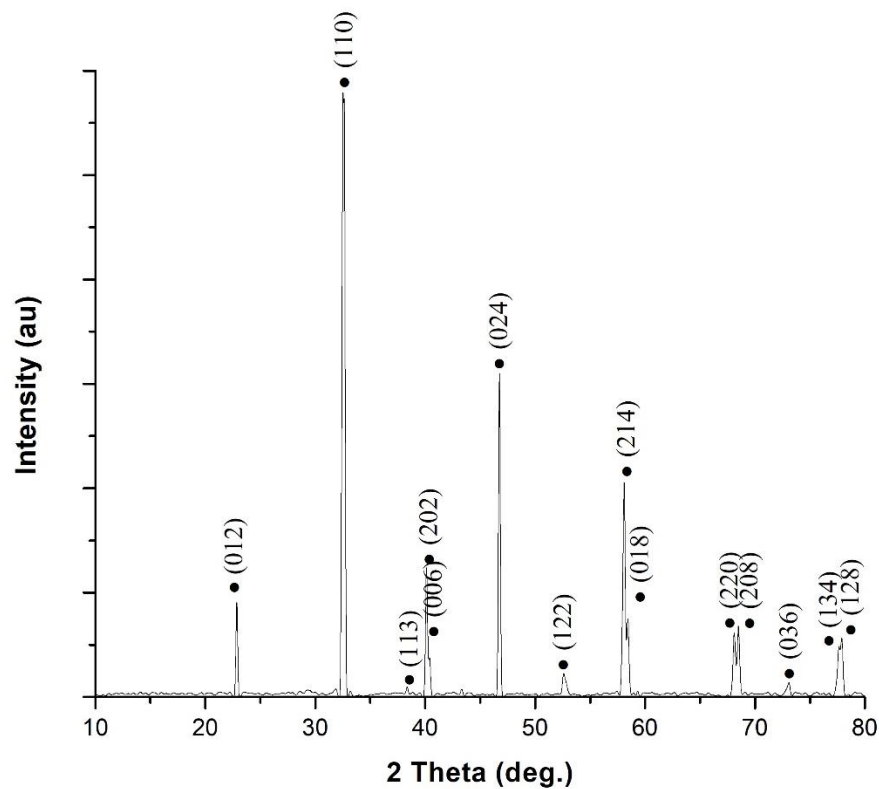

Figure 5.1: XRD pattern of the LSCF calcined at 800ºC for 5 hours

The crystallite size of the LSCF was calculated using the Scherrer equation which was 3.4 nm using FWHM of (1 1 0) diffraction peak.

$$D = \frac{0.9\lambda}{\beta \cos\theta} \dots\dots\dots\dots\dots\dots (5.1)$$

Where "λ" is the wavelength of x-ray which 1.54178, β is a full-width half-maximum of 110 peak which is 0.417, and "θ" is diffraction angle that is 16.304. The lattice parameter of LSCF is calculated by using the following equation which was 54.43nm:

$$a = d \sqrt{h^2 + k^2 + l^2} \dots\dots\dots(5.2)$$

5.1.2 Gadolinium doped Ceria ($Gd_{0.1}Ce_{0.9}O_{1.95}$)

Figure 5.2 shows the XRD pattern of gadolinium dope ceria calcined in air for 2 hours at 700°C for 2 hours which matches with JCPDS card #01-075-0161 [2]. Scherrer's equation 5.1 was used to calculate the crystallite size of the power which was 22.1nm.
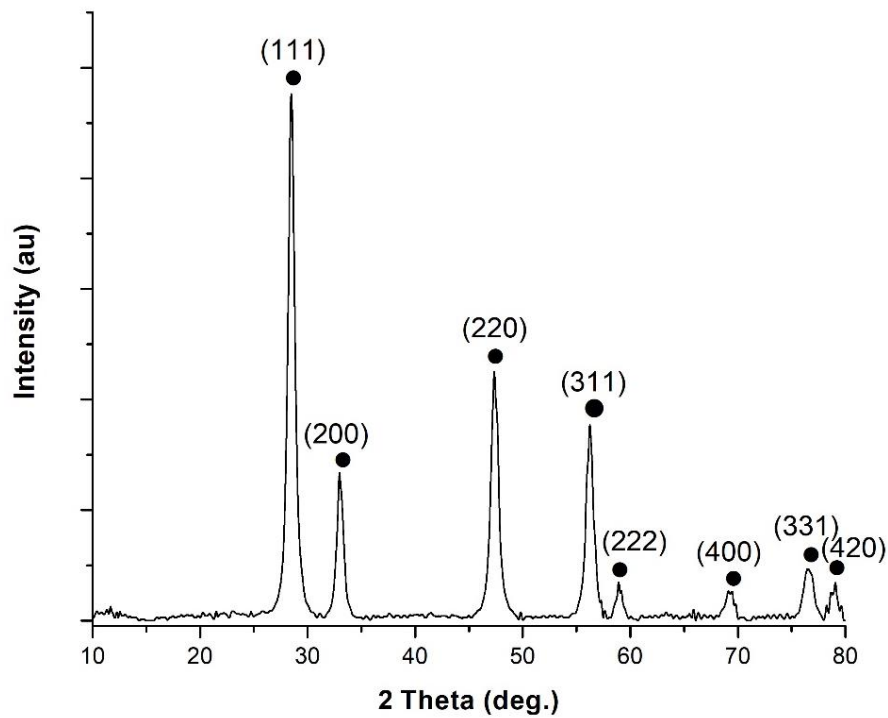

Figure 5.2: XRD pattern of GDC calcined at 700°C for 2 hours

5.1.3 LSCF-GDC Nanocomposite

Figure 5.3 shows the XRD pattern of LSCF-GDC composite synthesized by the solid-state route and sintered at 700°C for hours in the air.
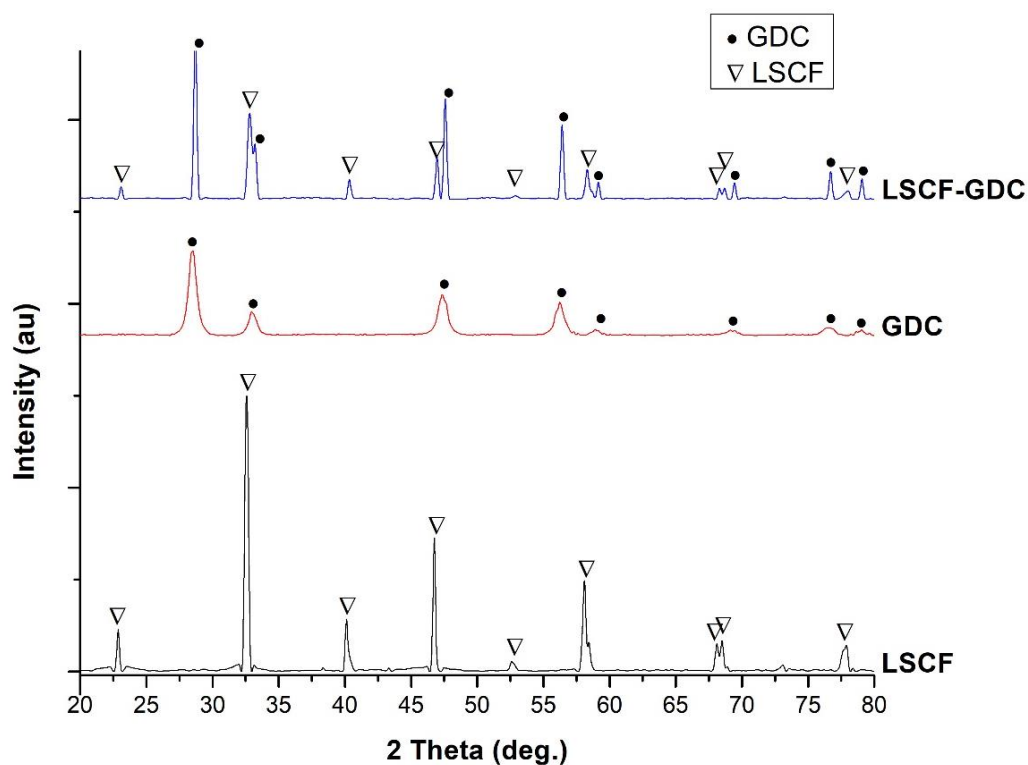

Figure 5.3: XRD Pattern of LSCF-GDC composite

5.2 Structural Analysis of LSCF-GDC Nanocomposite Cathode

5.2.1 Conventionally Sintered (CS) LSCF-GDC Nanocomposite Cathode

The cross-sectional analysis of the LSCF-GDC cathode pellet was performed using SEM. The cross-sectional images of conventionally sintered (CS) pellets sintered at 1100°C for 2 hours in the air are shown below in figure 5.4 and EDS analysis showed no elements were found except La, Sr, Co, Fe, Gd, Ce, and O which are the desired elements. EDS of conventionally sintered is shown in figure 5.5. The MS cathode was 97% dense assessed using ImageJ.
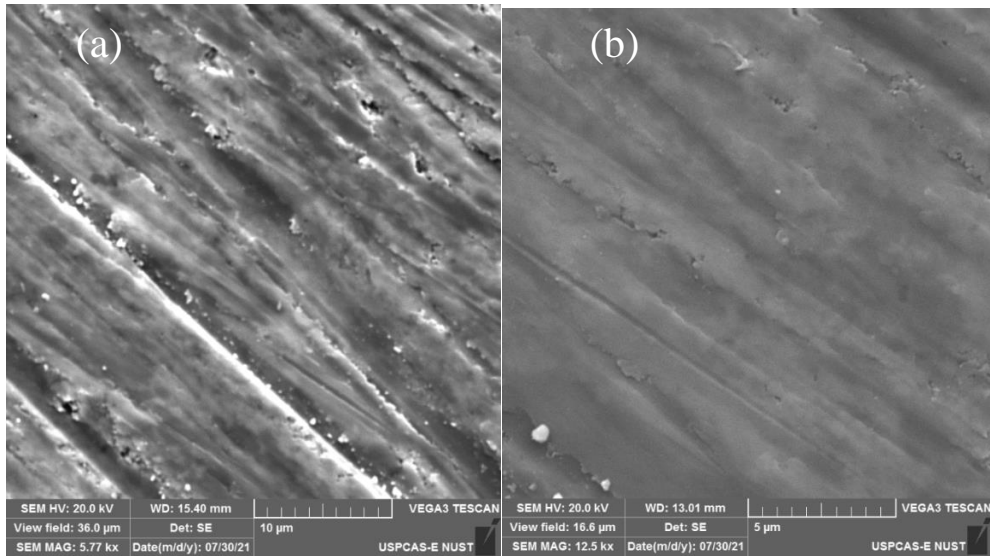
Figure 5.4: Cross-sectional image of the conventionally sintered (CS) LSCF-GDC nanocomposite cathode a) 10µm b) 5µm
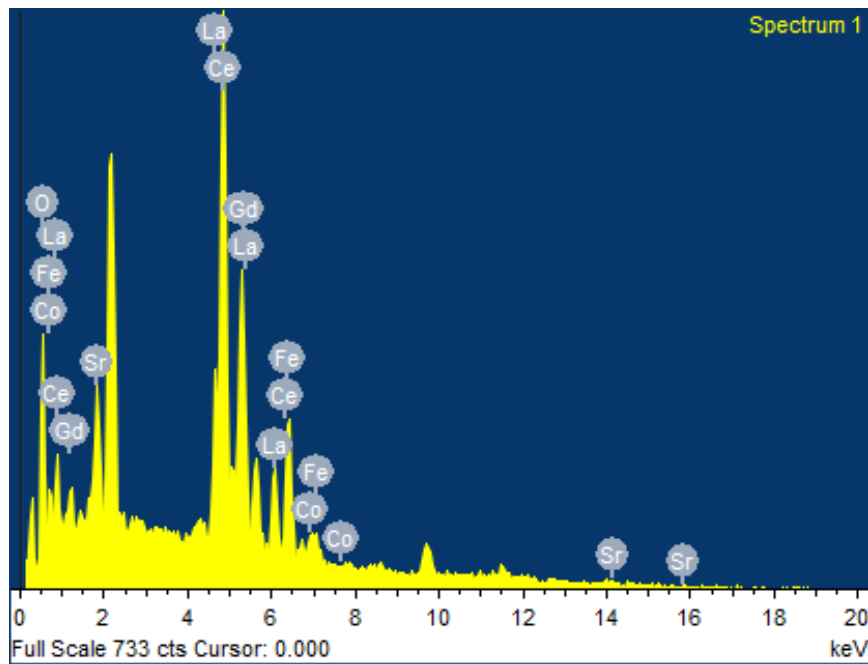

Figure 5.5: EDS of conventionally sintered LSCF-GDC nanocomposite cathode

5.2.2 Microwave Sintered (MS) LSCF-GDC Nanocomposite Cathode

A cross-sectional image of the microwave sintered (MS) pellet, which was sintered in a microwave furnace at 1100ºC at 10ºC/min for 2 hours is shown in fig 5.6 and EDS shows no other element besides the desired as shown in fig 5.7. The MS cathode was 95% dense assessed using ImageJ.
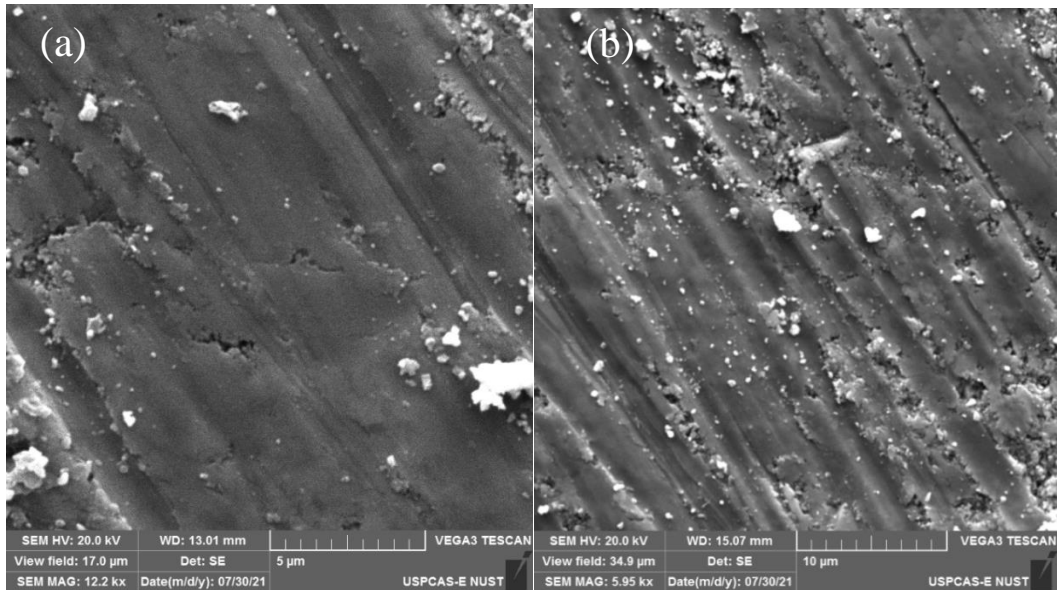
Figure 5.6: Cross-sectional image of the microwave sintered (MS) LSCF-GDC nanocomposite cathode a) 5µm b) 10µm
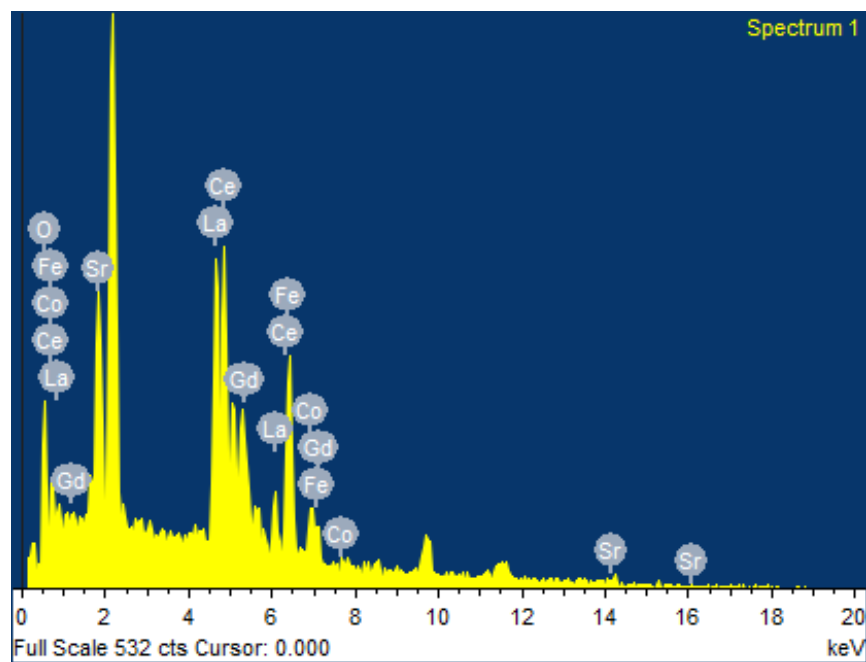

Figure 5.7: EDS of microwave sintered LSCF-GDC nanocomposite cathode

5.3 Electrical Properties of LSCF-GDC Nanocomposite Cathode

Electrical properties of the conventionally sintered and microwave sintered pellet were measured as a function of the temperature from 300°C to 600°C. The electrical

measurement was taken at a wide range of frequencies and the following equation was used to determine the ac conductivity of both CS and MS pellets.

$$\sigma_{ac} = 2\pi f \epsilon_o \epsilon' \tan\delta \dots\dots\dots\dots (5.3)$$

Where "σ_{ac}" is ac conductivity," $\tan\delta$" is tangent loss, "f" is frequency, "ϵ_o" is the permittivity of free space and "ϵ'" permittivity of material which can be found by the following equation:

$$\epsilon' = \frac{C \times d}{A \times \epsilon_o} \dots\dots\dots\dots\dots (5.4)$$

Where "C" is capacitance, "d" is the thickness of pellet, "A" is the area of pellet and "ϵ_o" is the permittivity of free space [4]. Figure 5.8 shows the calculated values of the conventionally and microwave sintered pellets are plotted against the temperature.
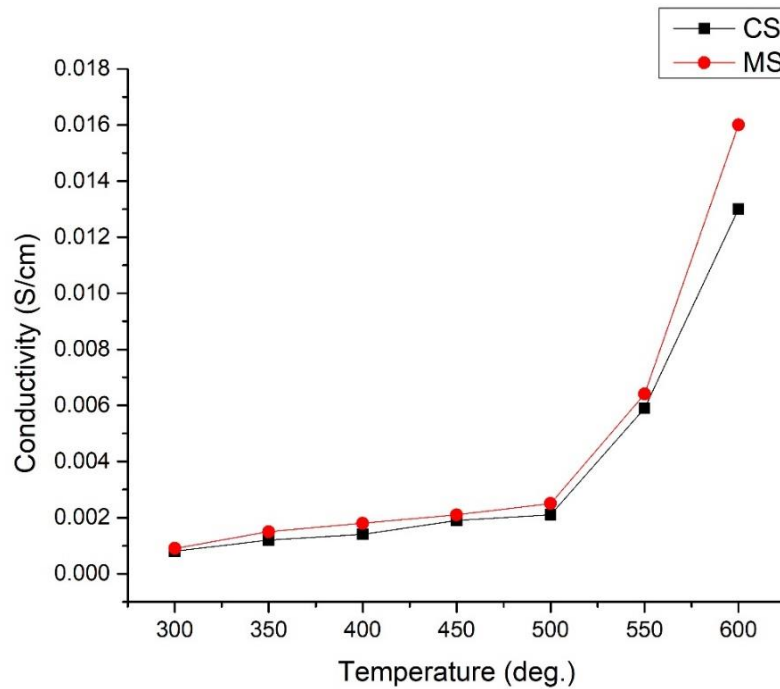

Figure 5.8: Conductivity of Microwave and conventionally sintered LSCF-GDC composite pellets

Table 5.2: Electrical Conductivities of LSCF-GDC nanocomposite cathode

Temperature (ºC)	Conductivity of Microwaved Sintered (S/cm)	Conductivity of Conventionally Sintered (S/cm)	Conductivity in Literature (S/cm) [1]
300	0.0009	0.0008	-
350	0.0015	0.0012	-
400	0.0018	0.0014	0.0013
450	0.0021	0.0019	0.0019
500	0.0025	0.0021	0.0020
550	0.0064	0.0059	0.0060
600	0.016	0.013	0.012

Microwave sintered cathode pellet showed a higher conductivity of 0.016 S/cm at 600ºC as compared to the conventionally sintered cathode, which is 0.013. The detail of the conductivities for conventionally and microwaved sintered pellets is shown in table 5.1. Microwave sintered pellets showed higher electrical conductivities at temperatures 300ºC to 600ºC. The conductivities of both tend to increase with the increase in temperature as an intrinsic behavior of the semiconductor [3].

Summary

The LSCF and GDC were successfully prepared as confirmed by XRD analysis. The XRD analysis of the LSCF-GDC nanocomposite cathode showed there were only individual XRD peaks of the LSCF and GDC suggesting that no chemical reaction occurred between LSCF and GDC and we can conclude that both are chemically compatible. The SEM analysis was used for cross-sectional analysis of both conventionally sinr=tered and microwave sintered cathodes. The images processing showed that the microwave sintered cathode was denser than the conventionally sintered cathode and exhibited higher electrical conductivity as compared to the conventionally sintered cathode at 600ºC.

References

[1]   A. P. Jamale, S. T. Jadhav, S. U. Dubal, C. H. Bhosale, and L. D. Jadhav, "Studies on the percolation limit of $Ce_{0.9}Gd_{0.1}O_{1.95}$ in $La_{0.6}Sr_{0.4}Co_{0.2}Fe_{0.8}O_{3-\delta}$-$Ce_{0.9}Gd_{0.1}O_{1.95}$ nanocomposites for solid oxide fuel cells application," *J. Phys. Chem. Solids*, vol. 85, pp. 96–101, 2015, doi: 10.1016/j.jpcs.2015.05.012.

[2]   L. D. Jadhav, M. G. Chourashiya, K. M. Subhedar, A. K. Tyagi, and J. Y. Patil, "Synthesis of nanocrystalline Gd doped ceria by combustion technique," *J. Alloys Compd.*, vol. 470, no. 1–2, pp. 383–386, 2009, doi: 10.1016/j.jallcom.2008.02.077.

[3]   S. A. Kumar, P. Kuppusami, and P. Vengatesh, "Auto-combustion synthesis and electrochemical studies of $La_{0.6}Sr_{0.4}Co_{0.2}Fe_{0.8}O_{3-\delta}$–$Ce_{0.8}Sm_{0.1}Gd_{0.1}O_{1.90}$ nanocomposite cathode for intermediate temperature solid oxide fuel cells," *Ceram. Int.*, vol. 44, no. 17, pp. 21188–21196, 2018, doi: 10.1016/j.ceramint.2018.08.164.

[4]   H. Bouaamlat *et al.*, "Dielectric Properties, AC Conductivity, and Electric Modulus Analysis of Bulk Ethylcarbazole-Terphenyl," *Adv. Mater. Sci. Eng.*, vol. 2020, 2020, doi: 10.1155/2020/8689150.

Chapter 6

Conclusions & Recommendations

6.1 Conclusions

LSCF and GDC powders were prepared through solution combustion synthesis. LSCF-GDC-nanocomposite was synthesized by mixing LSCF and GDC in a 1:1 ratio and sintering at 700°C for 2 hours. Nanocomposite cathode pellets were fabricated and sintered in conventional and microwave furnaces for the comparison of electrical properties. The following conclusions can be drawn:

1. The electronic conduction is dominant due to the presence of LSCF in the composite, which intrinsically has high electronic and low ionic conduction.
2. The electronic conduction increased with increasing the temperature, which was recorded from 300°C – 600°C. The microwave sintered (MS) cathode showed higher conductivity than the conventionally sintered (CS) cathode due to higher densification.
3. The LSCF-GDC composite is found to be a promising candidate for solid oxide fuel cell application as cathode material

6.2 Recommendations

The microwave sintering offered higher densification as compared to conventional sintering which in turn increased the electrical conductivity of LSCF- GDC cathode. The following recommendations can be drawn from the results.

1. A single cell with LSCF-GDC as cathode material can be fabricated and a comparison of electrochemical impedance spectroscopy (EIS) results between conventionally sintered and microwave sintered single cells can be done.
2. A comparison between microwave calcined and conventionally calcined LSCF and GDC powder can be done as microwave sintering offers better and uniform grain distribution.